N.M.R. in some antiferromagnetic hydrated complex Mn(II) chlorides

N.M.R. IN SOME ANTIFERROMAGNETIC HYDRATED COMPLEX Mn(II) CHLORIDES.

W.J.M. DE JONGE

N.M.R. IN SOME ANTIFERROMAGNETIC HYDRATED COMPLEX Mn(II) CHLORIDES.

PROEFSCHRIFT

TER VERKRIJGING VAN DE GRAAD VAN DOCTOR IN DE TECHNISCHE WETENSCHAPPEN AAN DE TECHNISCHE HOGESCHOOL TE EINDHOVEN OP GEZAG VAN DE RECTOR MAGNIFICUS PROF.DR.IR.A.A.TH.M. VAN TRIER, HOOGLERAAR IN DE AFDELING DER ELEKTROTECHNIEK, VOOR EEN COMMISSIE UIT DE SENAAT TE VERDEDIGEN OP DONDERDAG 9 APRIL DES NAMIDDAGS TE 4.00 UUR

DOOR

WILLEM JACOB MARINUS DE JONGE

GEBOREN TE LEEUWARDERADEEL

GREVE OFFSET NV – EINDHOVEN

DIT PROEFSCHRIFT IS GOEDGEKEURD DOOR DE PROMOTOR

PROF.DR. P. VAN DER LEEDEN.

CONTENTS

INTRODUCTION

This thesis deals with the experimental investigations on some antiferromagnetic complex hydrated manganese salts, such as $Cs_2MnCl_4.2H_2O$, $CsMnCl_3.2H_2O$ and $KMnCl_3.2H_2O$, with nuclear magnetic resonance (N.M.R)*. An advantage in the research on these Mn^{++} compounds is that the ground state of the Mn^{++} ion may be considered to a great extent as an S state, which leads to a mainly isotropic transfer interaction on the ligand ions. Our main concern will be the determination of the type of magnetic ordering, or the magnetic space group. In doing this we will need, apart from the proton resonance data, the information provided by the resonance on the ligand ion nuclei , i.c. the chlorines, and the cesium ion nuclei. The interpretation of the observed frequency spectrum of the nuclei of these ions is complicated by the fact that they possess an electric quadrupole moment which interacts with the electric field gradient tensors at the nuclear sites.

Therefore we will review in the first chapter the solutions of the Hamiltonian for combined Zeeman and quadrupole interactions as far as they will be needed in the interpretation. Chapter II will deal with the more specific problems which are encountered in the extraction of the information from the experimental data. After a general outline of the technical aspects of the experiments in chapter III, Chapter IV will be devoted to the description of a method for the determination of the electric field gradient tensor at a high field Cs site in $Cs_2MnCl_4.2H_2O$. In the last two chapters we will deal with the experimental investigations of the Mn^{++} salts mentioned above.

* A list of symbols and abbreviations can be found at the end of the thesis.

CHAPTER I

THEORY

1.1 Introduction

The Hamiltonian describing the interaction of a nucleus with spin quantum number $I \geq 1$, magnetic dipole moment $\vec{\mu}_n$ and electric quadrupole moment tensor $\vec{\vec{Q}}$ with a uniform magnetic field $\vec{B}$ and the crystalline electric field gradient tensor $\vec{\vec{\nabla E}}$ can be written as[1]

$$H = H_Z + H_Q$$

$$= -\vec{\mu}_n \cdot \vec{B} + \tfrac{1}{2}\vec{\vec{Q}} : \vec{\vec{\nabla E}} \qquad \text{(I-1)}$$

In this Hamiltonian, $\vec{B}$ stands for the total magnetic field at a nucleus and may contain, in general, the following contributions[2]

$$\vec{B} = \frac{\vec{\vec{A}} \cdot \langle \vec{S} \rangle}{\gamma_N \hbar} - 2\mu_B \langle r^{-3} \rangle \vec{L} + \vec{B}_{dipole} + \vec{B}_{ext} + \vec{B}_i' \qquad \text{(I-2)}$$

The first three terms represent respectively the spin hyperfine interaction, the orbital hyperfine interaction and the dipole interactions in the ordered state without an external field. The last two terms represent respectively the external field and the field-induced interactions. The prime on the last contribution serves to remind one that we are dealing with a paramagnetic, field-induced array of magnetic dipoles. In the paramagnetic state the first terms will be zero.
In the coordinate system, in which the electric field gradient tensor is diagonal, $-(\nabla E)_{ij} = V_{ij}\delta_{ij}$, and with

$$|V_{xx}| \leq |V_{yy}| \leq |V_{zz}| \ , \qquad \text{(I-3)}$$

(I-1) can be rewritten within the manifold of the 2I+1 substates of the spin quantum number I, as

$$H = -\gamma_N \hbar \vec{I} \cdot \vec{B} + \frac{e^2 qQ}{4I(2I-1)} \{3I_z^2 - \vec{I}^2 + \tfrac{1}{2}\eta(I_+^2 + I_-^2)\} \qquad \text{(I-4)}$$

I_z, $\vec{I}^2$, I_+, and I_- are angular momentum operators for the nucleus, η is the field gradient asymmetry parameter

$$\eta = (V_{xx} - V_{yy})/V_{zz}$$

and

$$eq = V_{zz} \quad .$$

In the case $I = 3/2$, (I-4) can be solved exactly only if the magnetic field lies along one of the principal axes of the electric field gradient tensor. This solution will be evaluated in the next paragraph.
Treating (I-4) with perturbation theory one has to distinguish between three cases:

a) The Zeeman interaction is large compared with the electric interaction, so H_Q may be treated as a perturbation. A discussion of this case has been given by Volkoff[3].
b) The Zeeman interaction is small compared with the electric interaction, so H_Z may be treated as a perturbation. This case was discussed by Pound[4], Ting[5] et al and Dean[6].
c) The Zeeman interaction is of the same order of magnitude as the electric interaction.

Apart from these, numerical solutions are available[7,8].
In this thesis we will deal with all three cases and in the following paragraphs we will give an outline of the theoretical results and derive those expressions suitable to the interpretation of the experimental results. Where the experimental part deals mainly with Cl^{35} nuclear resonance, we will limit ourselfs to the case in which $I = 3/2$.

1.2 Exact Solutions.

As has already been mentioned in the introduction, there is an exact solution of (I-1) if $\vec{B}$ is along one of the principal axes of the electric field gradient tensor. In this case the computation of the energy levels can be performed exactly by diagonalizing the two submatrices in the $|Im_z)$, $|Im_x)$ or $|Im_y)$ representations. The choice of the representation depends of course on the position of the magnetic field.

If we use for brevity:

$$F_x = \frac{-e^2qQ}{8I(2I-1)}(1-\eta) \qquad G_x = \frac{-e^2qQ}{8I(2I-1)}(3+\eta)$$

$$F_y = \frac{-e^2qQ}{8I(2I-1)}(1+\eta) \qquad G_y = \frac{e^2qQ}{8I(2I-1)}(3-\eta)$$

$$F_z = \frac{e^2qQ}{4I(2I-1)} \qquad G_z = \frac{e^2qQ}{4I(2I-1)}\eta \ ,$$

the Hamiltonian may be written as:

$$H = F_i(3I_i^2 - \vec{I}^2) + G_i(I_j^2 - I_k^2) \qquad \text{(I-5)}$$

in which i, j, k are x, y or z or a cyclic permutation of these; i denotes the chosen quantization axis.
The exact eigenvalues of (I-5) are (in frequency units)

$$E_{\pm\frac{3}{2}} = \mp\frac{\nu_Z}{2} + \frac{\nu_Q}{2}\left\{1+4\left\{\left(\frac{\nu_Z}{2}\right)^2 \mp 3\frac{\nu_Z}{2}F_i\right\}/\left(\frac{\nu_Q}{2}\right)^2\right\}^{\frac{1}{2}} \qquad \text{(I-6)}$$

$$E_{\pm\frac{1}{2}} = \mp\frac{\nu_Z}{2} - \frac{\nu_Q}{2}\left\{1+4\left\{\left(\frac{\nu_Z}{2}\right)^2 \mp 3\frac{\nu_Z}{2}F_i\right\}/\left(\frac{\nu_Q}{2}\right)^2\right\}^{\frac{1}{2}}$$

We have introduced :

$$\nu_Q = \nu_{Qo}\left(1+\frac{\eta^2}{3}\right)^{\frac{1}{2}} = \frac{3e^2qQ}{2I(2I-1)h}\left(1+\frac{\eta^2}{3}\right)^{\frac{1}{2}}$$

$$\nu_Z = \frac{\gamma_N}{2\pi}B,$$

which represent the frequencies of the transitions between the energy levels when respectively there is no magnetic interaction and there is no quadrupole interaction. We will use these abbreviations throughout this thesis. The expressions (I-6) are the same as given in Deans[6] article except for some minor errors.

1.3 High-field case.

For this problem it is convenient to choose the z axis along the magnetic field $\vec{B}$. The Hamiltonian (I-1) can then be transformed to the new coordinate system and takes the form

$$
\begin{aligned}
H = & - \gamma_N \hbar B I_z \\
& + \frac{e^2 qQ}{4I(2I-1)} \left[3I_x^2 \sin^2\theta + 3I_z^2 \cos^2\theta + \right. \\
& \qquad \left. - 3\sin\theta\cos\theta \, (I_x I_z + I_z I_x) - \vec{I}^2 \right] + \\
& + \frac{e^2 qQ\eta}{4I(2I-1)} \left[(I_x^2 \cos^2\theta - I_y^2 + I_z^2 \sin^2\theta) \cos 2\phi + \right. \\
& \qquad -(I_x I_y + I_y I_x) \cos\theta \sin 2\phi + \\
& \qquad -(I_y I_z + I_z I_y) \sin\theta \sin 2\phi + \\
& \qquad \left. +(I_z I_x + I_x I_z) \sin\theta\cos\theta\cos 2\phi \right] .
\end{aligned}
\qquad \text{(I-7)}
$$

The ϕ and θ in (I-7) are respectively the azimuthal and polar angle of the magnetic field with respect to the principal axes of the electric field gradient.

Introducing for brevity $a = I(I+1)$, we obtain for the matrix elements $(Im_I | H | Im_I') = H_{mm'}$ of H in the $|Im_I)$ representation (in frequency units):

$$
\begin{aligned}
H_{mm} &= - \nu_Z m + \frac{\nu_{Qo}}{4} \left(m^2 - \frac{1}{3} a \right) (3\cos^2\theta - 1 + \eta \sin^2\theta \cos 2\phi) \\
H_{m,m+1} &= H^*_{m+1,m} \\
&= - \frac{\nu_{Qo}}{4} \left\{ (2m+1)(I-m)^{\frac{1}{2}} (I+m+1)^{\frac{1}{2}} \right\} \sin\theta \\
&\qquad \left\{ \cos\theta - \frac{1}{3} \eta (\cos\theta\cos 2\phi - i \sin 2\phi) \right\} \qquad \text{(I-8)} \\
H_{m,m+2} &= H^*_{m+2,m} \\
&= \frac{\nu_{Qo}}{8} \left\{ (I-m-1)(I-m)(I+m+1)(I+m+2) \right\}^{\frac{1}{2}} \\
&\qquad \left\{ \sin^2\theta + \frac{1}{3} \eta (1+\cos^2\theta) \cos 2\phi - \frac{2}{3} i \eta \cos\theta \sin 2\phi \right\} .
\end{aligned}
$$

Standard perturbation theory, treating the quadrupole interaction as a perturbation, gives for the energies correct to second order

$$E = E_m^o + E_m^1 + E_m^2 \ldots.$$

$$E_m^o = - \nu_Z m$$

$$E_m^1 = \frac{\nu_{Qo}}{4} (m^2 - \tfrac{1}{3}a)(3\cos^2\theta - 1 + \eta \sin^2\theta\cos 2\phi)$$

$$E_m^2 = - \frac{\nu_{Qo}^2}{8\nu_Z} m(8m^2-4a + 1) \sin^2\theta\{\cos^2\theta - \tfrac{2}{3} \eta \cos^2\theta\cos 2\phi + \tfrac{1}{9} \eta^2(1 - \sin^2\theta\cos^2 2\phi)\} + \quad \text{(I-9)}$$

$$- \frac{\nu_{Qo}}{32\nu_Z} m(-2m^2 + 2a - 1)\{\sin^4\theta + \tfrac{2}{3} \eta \sin^2\theta(1+\cos^2\theta)\cos 2\phi + \tfrac{1}{9} \eta^2(4\cos^2\theta + \sin^4\theta\cos^2 2\phi)\} .$$

If $\nu_Z >> \nu_Q$ the m are almost good quantum numbers and the energy levels may therefore be characterised by m. The transitions we can observe are therefore (with the selection rule $\Delta m = \pm 1$) the transitions between adjacent levels. For the case where I = 3/2 the energy level scheme in a high magnetic field is given in figure I-1 .We will observe three transitions which will be labeled ν_1, ν_2 and ν_3. The transition $|-\tfrac{1}{2}) \leftrightarrows |+\tfrac{1}{2})$ will play a dominant part in the following sections and we will mark it as ν_2.

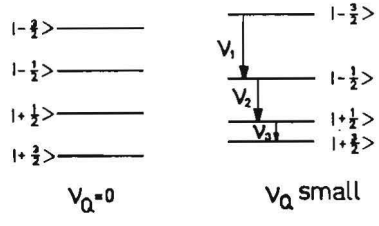

Fig.I-1 Energy level scheme for a chlorine nucleus subjected simultaneously to a high magnetic field and a relatively small quadrupole interaction. Arrows indicate the observable transition.

Expressions for ν_i as a function of θ, η and ϕ can in general be obtained from (I-9). They will not be given here. An illustration of the behaviour of ν_i as function of θ for several values of η and ϕ is given in figure I-2, where we characterise the curves by the value of $\eta\cos 2\phi$, neglecting the terms with η^2.

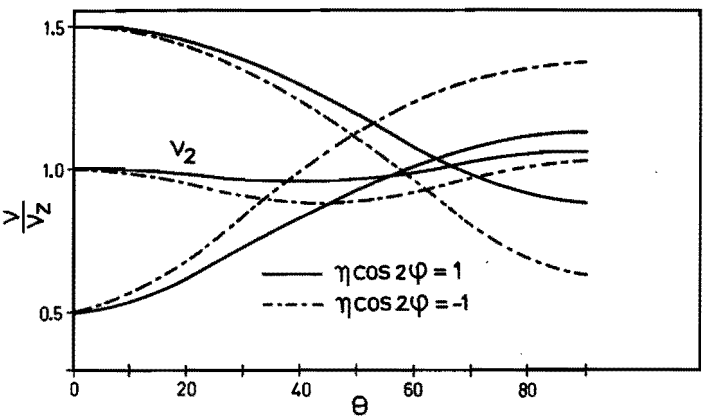

Fig.I-2 Illustration of the behaviour of ν_i as function of θ for several values of $\eta\cos 2\phi$ in the high field case.

In figure I-3 a graphical comparison is made between the exact computer solutions for ν_i and the frequencies obtained from (I-9), for the case in which $\frac{\nu_Z}{\nu_{Qo}} = 2$, $\eta = 0.5$ and $\phi = 0$. Even in this situation where we can hardly speak of a high field case ($\frac{\nu_Z}{\nu_{Qo}}$ is only 2) the agreement is quite satisfactory. As the deviations will decrease with decreasing $\frac{\nu_{Qo}}{\nu_Z}$ and η, we may expect that for not too big η and not too small $\frac{\nu_Z}{\nu_{Qo}}$ the frequencies derived from (I-9) give a fairly good description of the behaviour of the frequencies as a function of θ, η and ϕ .
The angles at which ν_1 and ν_3 coalesce are found to be from (I-9)

$$3\cos^2\theta - 1 + \eta \sin^2\theta\cos 2\phi = 0. \qquad \text{(I-10)}$$

This equation describes an elliptical cone in space. If we are able to trace this cone experimentally, its major and minor axes will give the principal axes of the electric field gradient and from its conical angles

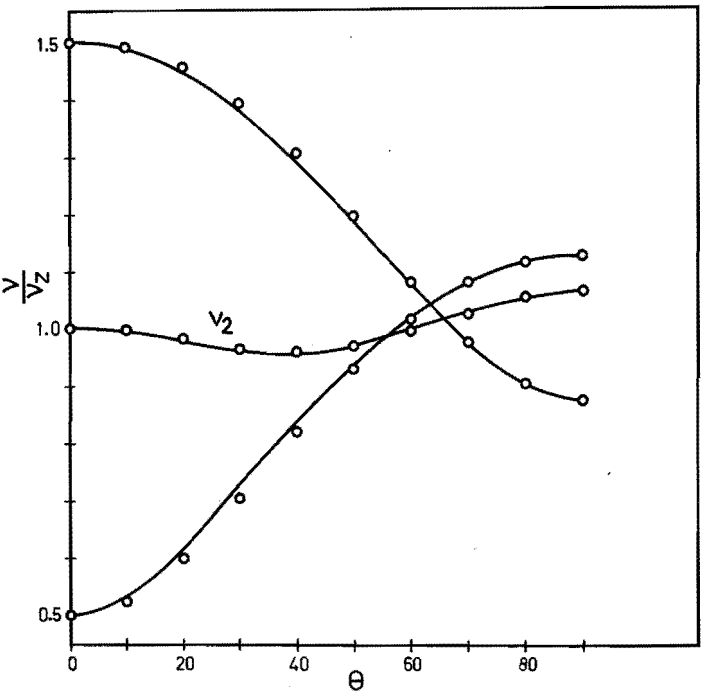

Fig.I-3 Graphical comparison between the exact computor solutions (the drawn curve) and second order perturbation theory (the data points) for the case where $\nu_Z/\nu_{Qo} = 2$, $\eta = 0.5$ *and* $\phi = 0$.

it is possible to determine the asymmetry parameter η. This question will be discussed in detail in chapter IV. Although (I-10) is in general valid only up to second order in ν_{Qo}, we will prove that in the case of I = 3/2 it is an exact solution (section 4.2).

1.4 Low-field case.

For this problem we choose the coordinate system in which $\vec{\vec{V}}\vec{E}$ is diagonal, that is the x, y and z axes fall along the principal axes of the electric field gradient tensor.
In this coordinate system the Hamiltonian (I-1) can be written as:

$$H = H_Q + H_Z$$

with

$$H_Q = \frac{e^2qQ}{4I(2I-1)} \{3I_Z^2 - \vec{I}^2 + \tfrac{1}{2}\eta(I_+^2 + I_-^2)\} \qquad \text{(I-11)}$$

$$H_Z = -\gamma\hbar B\{I_Z\cos\theta + \tfrac{1}{2}\sin\theta(I_+e^{-i\phi} + I_-e^{+i\phi})\}.$$

If the magnetic field at the nucleus under consideration is zero then $H = H_Q$ and for $I = 3/2$ an exact solution can be found:

$$E_{\pm} = \pm \frac{3e^2qQ}{4I(2I-1)} \left(1 + \frac{\eta^2}{3}\right)^{\frac{1}{2}} . \qquad \text{(I-12)}$$

Both energy levels are doubly degenerate. Transitions $|\Delta\tilde{m}| = 1,2$ give rise to one frequency ν_Q

$$\nu_Q = \frac{3e^2qQ}{2I(2I-1)h} \left(1 + \frac{\eta^2}{3}\right)^{\frac{1}{2}} = \nu_{Qo}\left(1 + \frac{\eta^2}{3}\right)^{\frac{1}{2}} . \qquad \text{(I-13)}$$

The eigenfunctions belonging to the eigenstates (I-12) are

$$\begin{aligned}
|+\tilde{\tfrac{3}{2}}) &= A|+\tfrac{3}{2}) + B|-\tfrac{1}{2}) \\
|-\tilde{\tfrac{3}{2}}) &= A|-\tfrac{3}{2}) + B|+\tfrac{1}{2}) \qquad \text{(I-14)} \\
|+\tilde{\tfrac{1}{2}}) &= C|+\tfrac{1}{2}) + D|-\tfrac{3}{2}) \\
|-\tilde{\tfrac{1}{2}}) &= C|-\tfrac{1}{2}) + D|+\tfrac{3}{2})
\end{aligned}$$

in which

$$A = \eta\{3(\frac{\eta^2}{3} + (1-\rho)^2)\}^{-\frac{1}{2}} \qquad B = (\rho-1)\{\frac{\eta^2}{3} + (1-\rho)^2\}^{-\frac{1}{2}}$$

$$C = (\rho+1)\{\frac{\eta^2}{3} + (1+\rho)^2\}^{-\frac{1}{2}} \qquad D = -\eta\{3(\frac{\eta^2}{3} + (1+\rho)^2)\}^{-\frac{1}{2}}$$

$$\rho = (1+\frac{\eta^2}{3})^{\frac{1}{2}}.$$

After expressing the H_z in this basis, the first order correction of the energy can be found by diagonalizing the Zeeman perturbation in each pair of degenerate states.

This leads to the following expressions for the energy levels (in frequency units):

$$E_{\pm\frac{3}{2}} = \tfrac{1}{2}\nu_Q \mp \frac{\nu_Z}{2}\left\{\cos^2\theta\left(1+\frac{2}{\rho}\right)^2 + \sin^2\theta\left\{\left(\frac{\eta}{\rho}\right)^2+\left(1-\frac{1}{\rho}\right)^2 + 2\frac{\eta}{\rho}\left(1-\frac{1}{\rho}\right)\cos 2\phi\right\}\right\}^{\frac{1}{2}}$$

$$E_{\pm\frac{1}{2}} = -\tfrac{1}{2}\nu_Q \mp \frac{\nu_Z}{2}\left\{\cos^2\theta\left(\frac{2}{\rho}-1\right)^2 + \sin^2\theta\left\{\left(\frac{\eta}{\rho}\right)^2+\left(1+\frac{1}{\rho}\right)^2 - 2\frac{\eta}{\rho}\left(1+\frac{1}{\rho}\right)\cos 2\phi\right\}\right\}^{\frac{1}{2}} \qquad \text{(I-15)}$$

Generally there are four transitions which can be observed. They are shown in figure (I-4).

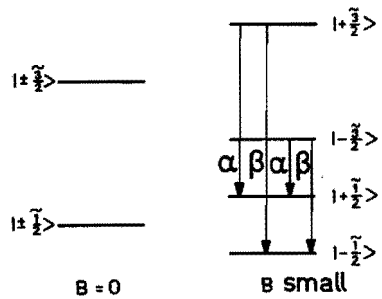

Fig.I-4 The energy level scheme for a chlorine nucleus subjected simultaneously to an electric field gradient and a relatively small magnetic field $\vec{B}$.

We will call the pair with the larger frequency separation the β pair, and the pair with smaller frequency separation the α pair. Because of the general mixing of the states by the asymmetry parameter η and the magnetic field, we will observe both α and β lines with varying intensities depending on the orientation of the magnetic field. For a detailed analysis of this problem the reader is referred to Dean's article[6].

1.5 Intermediate case.

If the Zeeman interaction and the quadrupole interaction are of the same order of magnitude, the mixing of the states will be strong and m will be no longer a good quantum number, consequently we will be able to see transitions between all the energy levels. Of course the transition frequencies will be related to each other by sum rules.

1.6 Method of moments.

Brown and Parker[9] and Parker and Spence[10] developed a method based on the moments of the energy, defined by $\Gamma_n = \sum_i (E_i)^n$, which has a great bearing on the interpretation of the nuclear resonance pattern in mixed cases. The eigenvalues of the Hamiltonian (I-4) are the roots of the secular equation. In the case of $I = \frac{3}{2}$ this is a polynomial of the fourth degree in E

$$E^4 + a_1E^3 + a_2E^2 + a_3E + a_4 = 0 \ .$$

The coefficient a_r can be expressed in the eigenvalues E_i as:

$$\begin{aligned} a_1 &= -\sum_i E_i \\ a_2 &= \sum_i \sum_j E_iE_j \qquad i < j \\ a_3 &= -\sum_i \sum_j \sum_k E_iE_jE_k \qquad i < j < k \\ a_4 &= E_1E_2E_3E_4 \ . \end{aligned} \tag{I-16}$$

Because of the fact that the Hamiltonian describing the system is traceless, (I-16) can be written as

$$\begin{aligned} a_1 &= 0 \qquad\qquad = \Gamma_1 \\ a_2 &= -\tfrac{1}{2}\sum_i (E_i)^2 = -\tfrac{1}{2}\Gamma_2 \\ a_3 &= -\tfrac{1}{3}\sum_i (E_i)^3 = -\tfrac{1}{3}\Gamma_3 \\ a_4 &= \frac{\Gamma_2^2 - 2\Gamma_4}{8} \ . \end{aligned} \tag{I-17}$$

It can be shown that for I = 3/2 the secular equation of (I-4) can be written , without any approximation, as:

$$\begin{aligned} &E^4 - \{\frac{5}{2}\nu_Z^2 + \frac{\nu_{Qo}}{2}(1 + \frac{\eta^2}{3})\}E^2 + \\ &- \frac{\nu_{Qo}\nu_Z^2}{3}(3\cos^2\theta - 1 + \eta \sin^2\theta\cos 2\phi)\ E + \\ &+ \nu_{Qo}^4(1 + \frac{\eta^2}{3})^2 + \frac{\nu_Z^2\nu_{Qo}^2}{8}\{6\sin^2\theta(1-\tfrac{\eta^2}{3}) - 5 + \eta^2 + 4\eta\sin^2\theta\cos 2\phi\} \\ &+ \frac{9}{16}\nu_Z^4 = 0 \ . \end{aligned} \tag{I-18}$$

So the expressions for the energy moments are:

$$\Gamma_1 = 0$$

$$\Gamma_2 = 5\nu_Z^2 + \nu_{Qo}^2(1 + \frac{\eta^2}{3}) \qquad \text{(I-19)}$$

$$\Gamma_3 = \nu_{Qo}\nu_Z^2(3\cos^2\theta - 1 + \eta \sin^2\theta\cos 2\phi).$$

In every practical case where we can construct an energy level scheme from the experimental data, (I-19) gives a relation between the experimental observable frequencies and the unknown ν_Z, ν_{Qo}, η, θ and ϕ. Furthermore application of $\vec{\nabla}_B$, defined as $\vec{\nabla}_B = \vec{i}\frac{\partial}{\partial B_x} + \vec{j}\frac{\partial}{\partial B_y} + \vec{k}\frac{\partial}{\partial B_z}$ on the energy moments gives a useful relation between the experimental quantities $\vec{\nabla}_B\nu_i$ and the local field direction $\vec{B}$.
If we define :

$$\nu_i = (E_{i+1} - E_i)/h$$

then, if $\Gamma_1 = 0$,

$$E_n = \sum_{i=1}^{n-1} \frac{i}{2I+1}\nu_i + \sum_{i=n}^{2I}(-1 + \frac{i}{2I+1})\nu_i$$

$$= \sum_{i=1}^{2I} c_i(n)\nu_i$$

where

$$c_i(n) = \frac{i}{2I+1} \quad \text{if } 1 \le i \le n-1$$

$$c_i(n) = -1 + \frac{i}{2I+1} \quad \text{if } n \le i \le 2I$$

and

$$\Gamma_2 = \sum_{n=o}^{2I}\sum_{i=1}^{2I}\sum_{j=1}^{2I} c_i(n)\, c_j(n)\nu_i\nu_j \qquad \text{(I-20)}$$

$$\Gamma_3 = \sum_{n=o}^{2I}\sum_{i=1}^{2I}\sum_{j=1}^{2I}\sum_{k=1}^{2I} c_i(n)\, c_j(n)\, c_k(n)\nu_i\nu_j\nu_k. \qquad \text{(I-21)}$$

(I-20) and (I-21) combined with (I-19) give a relation between the observed frequencies and the unknown interaction parameters. Application of $\vec{\nabla}_B$ on (I-20) and (I-21) gives:

$$\vec{\nabla}_B \Gamma_2 = \sum_{n=o}^{2I} \sum_{i=1}^{2I} \sum_{j=1}^{2I} c_i(n)\, c_j(n) \nu_1 \vec{\nabla}_B \nu_j \qquad \text{(I-22)}$$

$$\vec{\nabla}_B \Gamma_3 = \sum_{n=o}^{2I} \sum_{i=1}^{2I} \sum_{j=1}^{2I} \sum_{k=1}^{2I} c_i(n)\, c_j(n)\, c_k(n)\, \nu_i \nu_j \vec{\nabla}_B \nu_k \,. \qquad \text{(I-23)}$$

From (I-19) we can evaluate,

$$\vec{\nabla}_B \Gamma_2 = 5\left(\frac{\gamma}{2\pi}\right)^2 \vec{B}_1 \cdot \{ \vec{\nabla}_B \vec{B}_1 + (\vec{\nabla}_B \vec{B}_1)_t \} \,, \qquad \text{(I-24)}$$

where the subscript t means transposed. (I-24) links the theoretical expressions for $\vec{\nabla}_B \Gamma_2$ to the experimental reality. The gradient $\vec{\nabla}_B$ can only be determined with the aid of an external field $\vec{B}$. The influence of $\vec{B}$ on the internal local field $\vec{B}_1$ is given by the so called field-shift tensor [11,12,13] which arises from the field-induced effects in the Hamiltonian (I-2). As can be seen from (I-24) and (I-2), the effect of the field shift tensor can be characterised by a symmetric second-rank tensor which contains symmetrized products of both the hyperfine tensor $\vec{\vec{A}}$ and the dipole tensor $\vec{\vec{\Delta}}$ with the single ion susceptibility tensor $\vec{\vec{\chi}}$[13]. We will refer to this expression in the next chapter (section 2.4) where we will discuss the determination of the direction of the local magnetic field at a nucleus.

CHAPTER II

EXPERIMENTAL METHODS

2.1 Introduction

In this chapter we will give some details about the techniques used in our experiments to obtain and interpret the experimental data.
The main problems will be the determination of the magnetic space group of the crystal in the antiferromagnetic state, and how to extract the vital information such as the magnitude and direction of the hyperfine fields at the ligand nuclei from the frequency spectrum.

2.2 The determination of the magnetic space group.

The magnetic space group leaves the spatial arrangement of magnetic moments invariant, as the crystallographic space group leaves only the position of the atoms invariant. The magnetic space groups are identical with the colored and uncolored Shubnikov groups and are usually described by this name.
Apart from crystallographic group elements which, however, in the magnetic space group act also on axial vectors as magnetic moments and magnetic fields, the Shubnikov group may contain group elements which are products of the aforementioned elements and a color or time inversion operator 1'. These operators, which are denoted by an accent on the "normal" operators, reverse the axial vector under consideration. It is clear that a magnetic field at two crystallographic equivalent positions related by the symmetry operator A will still be equal in magnitude but the operator which relates the two directions may be A or A'. Opechowski[33] has given a convenient listing of all the magnetic space groups compatible with a certain crystallographic space group. However, it should be noted that the magnetic space group describing a certain magnetic ordening at low temperatures is not always one of the Shubnikov groups belonging to the Opechowski family of the crystallographic space group of the crystal. The reason for this is that one or more crystallographic symmetry elements present in the paramagnetic state may have disappeared in the ordered state[14,15].

Because of this, the best procedure in selecting the magnetic space group is not to start the selection with the crystallographic symmetry, but with the experimentally observed symmetry of the local fields and to eliminate all the magnetic point groups which do not lead to this symmetry. A further selection of the magnetic point group can then be made by comparing the number of nuclei under consideration with the number of distinct field magnitudes found at these nuclei and the number of different field directions belonging to one particular field magnitude. At this point something should be said about the action of a symmetry operator on an axial vector. This can be visualized by treating the axial vector as a circular current. The main point is that an axial vector is invariant under inversion. This means that under product operations $\bar{R} = R \cdot i$ an axial vector behaves the same as a positional or polar vector under the operation R. Table III-1 gives a similar transformation for all the magnetic point symmetry operators.

Table III-1 . Correspondence between the action of point symmetry operators on axial and polar vectors.

axial	polar equivalent	axial	polar equivalent
E	E	E'	$\bar{E}$
$\bar{E}$	E	$\bar{E}$'	$\bar{E}$
2	2	2'	$\bar{2}$
$\bar{2}$	2	$\bar{2}$'	$\bar{2}$
3	3	3'	$\bar{3}$
$\bar{3}$	3	$\bar{3}$'	$\bar{3}$
4	4	4'	$\bar{4}$
$\bar{4}$	4	$\bar{4}$'	$\bar{4}$
6	6	6'	$\bar{6}$
$\bar{6}$	6	$\bar{6}$'	$\bar{6}$

The experimentally observed directions of the local fields at the sites of the nucleus under study (for instance the protons) reveal a symmetry which is not the magnetic point symmetry of the crystal, but its polar analogon[34]. Spence et al[20] introduced the name aspect group for this symmetry.

With the aid of table III-1 it is possible to determine the aspect group which will be generated by any Heesch group. Van Dalen[16] tabulated the Heesch groups which are compatible with a certain aspect group. With those tables we are able to select those Heesch groups which could lead to the experimentally observed symmetry of the aspect group. A further selection of the possible Heesch groups is based on the following two arguments:

1) Because of the fact that an inversion operator leaves an axial vector invariant, the presence of an inversion operator in the Heesch group will not reveal itself in the symmetry elements of the aspect group. So if N_a is the number of elements in the aspect group and N_h the number of elements in the Heesch group, we may conclude that N_a equals $\frac{1}{2}N_h$ or N_h depending on whether the Heesch group does or does not contain the inversion operator.
2) Since we are dealing with point groups let us consider the number nuclei of a certain kind, c.q. protons, in a chemical unit cell which are <u>not</u> related by a translation operator. We will call this number N_n. In the case of a primitive lattice N_n will equal the total number of protons in the cell, or the number of protons per lattice point. In the case of a centered cell it is merely the number of protons per lattice point. If the Heesch group does <u>not</u> contain the anti-identity separately, that is if the Shubnikov group does <u>not</u> contain an anti-translation, it will be clear that N_n divided by the number of observed distinct local field magnitudes at proton sites N_f will equal N_h.
   If the Heesch group does contain the anti-identity, so the Shubnikov group contains one or more anti-translations, the original Bravais lattice points are no longer magnetically equivalent but the lattice can be divided in a colored and an uncolored one. That is

$$\frac{2N_n}{N_f} = N_h \text{ or } \frac{N_n}{N_f} = \frac{N_h}{2} \quad .$$

Combining the arguments given above we arrive at a set of selection rules given below. These rules are similar to those given by Spence and Van Dalen[17]. A correction has been made in their definitions of N_n, where the phrase "equivalent nuclei in the chemical unit cell" may give rise to misunderstanding especially when one deals with centered lattices. Let N_a be the number of elements in the aspect group, N_f the

number of observed distinct field magnitudes at the site of a particular nucleus and N_n the total number of nuclei under study in the chemical unit cell which are not related by a translation operator. We can now distinguish the following cases:

1) $N_a N_f / N_n = \frac{1}{2}$: the magnetic space group contains the inversion and the magnetic unit cell is identical with the chemical unit cell (The magnetic space group contains no anti-translation.).
2) $N_a N_f / N_n = 2$: the magnetic space group does not contain the inversion and the magnetic unit cell is not identical with the chemical unit cell (The magnetic space group contains at least one anti-translation).
3) $N_a N_f / N_n = 1$: the magnetic space group contains both an inversion and an anti-translation or it contains neither an inversion nor an anti-translation.

The selection of the Shubnikov groups is completed with a comparison of the obtained magnetic point groups with the room temperature chemical space group. One has to add the translational components to the magnetic point group that is transfer mirrorplanes to glide planes etc. in such a way that the Shubnikov group does relate the appropriate positions. In doing this we assume that the nature of the point symmetry operators , as far as they still exist in the anti-ferromagnetic state, has not changed. In general there is more than one possible space group when this selection is completed. A decision between these can be based on a check whether the orientation of the magnetic fields $\vec{B}$ or magnetization $\vec{M}$ at nuclei or ions occupying special positions are in agreement with the orientations allowed at these positions by the magnetic space group. In table III-2 the allowed orientations of $\vec{B}$ and $\vec{M}$ on special positions are tabulated. A second check can be found in a comparison of a dipole calculation for each of the possible structures with the experimentally obtained local dipole fields.

As has already been mentioned, the selection procedure outlined above provides a convenient way of finding the magnetic space group, even when one or more point symmetry elements have disappeared in the ordered state. However, it should be noted that changes which affect the lattice in such a way that the number of nuclei per lattice point alters, may lead to a wrong selection of the magnetic space group. Therefore, one should allow N_n to be a multiple of the value obtained from the room temperature crystallographic data in those cases when one is not sure whether such a crystallographic change has taken place.

Table III-2. Allowed orientations of axial vectors on special positions.

local point operator*	allowed direction of $\vec{B}$ or $\vec{M}$
R_z ; $\bar{R}_z$	(o,o,z)
R'_z ; $\bar{R}'_z$	(x,y,o)
E' ; $\bar{E}'$	none
R_{zt} ; $\bar{R}_{zt}$	any
R'_{zt} ; $\bar{R}'_{zt}$	any
E ; $\bar{E}$	any

* $R_z, \bar{R}_z, R_{zt}$ are respectively the rotation operator, the rotation inversion operator and the rotation operator combined with a translation, all along the z axis.

2.3 Determination of the proton positions

X-ray determinations of the crystallographic structure and the atomic parameters in general do not give more than a suggestion (if any) of the proton positions in the water of hydration. Because these positions must be known before a dipole calculation of the magnetic field on these protons can be performed it is sometimes necessary to find some experimental evidence for the suggested positions or even determine the positions by alternate methods. In the following we will give a brief review of the methods which were applied in the research described in this thesis. For a more detailed description the reader is referred to the original papers.

1) Pake[35] has shown by means of perturbation theory that the splitting of the lines, $\Delta\nu$, for an identical isolated pair of protons (as can be found in a water molecule) in a magnetic field is given by

$$\Delta\nu = \frac{\gamma}{2\pi} 3 \frac{\mu_p}{r^3} (3\cos^2\theta - 1), \qquad \text{(II-1)}$$

where μ_p is the magnetic moment of the proton and θ the angle between the p-p vector $\vec{r}$ and the external magnetic field.
A resonance diagram obtained by plotting the angular dependence

of the absorption frequencies will thus yield a value for the p-p - distance and the direction of the p-p vector. When the oxygen positions are known, these data are usually sufficient to locate the protons quite accurately[27].

2) Baur[28] expressed the view that the orientation of the water molecule is determined by the electrostatic interactions between the water molecules and the surrounding atoms. This view is supported by the good agreement found in several hydrates between the positions of the hydrogen atoms as determined by neutron diffraction and as calculated theoretically to have the least electrostatic energy.
A computor programme for the calculation of least electrostatic energy written by Hijmans[37] was found to give excellent agreement with the earlier calculations of Baur ; we used this programme in the case of $KMnCl_3{}^2H_2O$.

3) If one substitutes deuterium in the hydrated compounds one may draw conclusions about the orientations of the D_2O molecule from the orientation of the principal axes of the electric field gradient tensor on the deuterium sites .
If we neglect the small dipole-dipole interaction, the relevant formulae which describe the splitting of the absorption line of deuterium in a high field as a function of the rotation angle of the crystal about any axis perpendicular to the magnetic field are given by Volkoff[3,30].

$$\Delta\nu = \frac{3}{8}\,\frac{eQ}{h}\,\{V_{zz} - (V_{xx} - V_{yy})\cos 2\theta + V_{xy}\sin 2\theta\} \quad .(II\text{-}2)$$

The V_{ij} are components of the field gradient tensor in the coordinate system fixed on the crystal. The rotation axis is along the z-axis , and θ is zero when the magnetic field coincides with the x-axis. Similar expressions for rotations about the x-and y-axis may be obtained by cyclic permutation of the subscripts. From several rotations about different axis one may deduce the components V_{ij}. Diagonalization of the obtained matrices will yield the principal axes of the electric field gradient tensor at the deuterium nuclei. Several authors[38,39] have pointed out that there exist a relation between the orientation of the D_2O molecule and the principal axes. The z-axis of the field gradient is in general within a few degrees along the O-D bond, while the y-axis is almost perpendicular to the D-O-D. plane.

So the knowledge of the principal axes may give an indication of the positions of the deuterium atoms and also of the protons if we assume that the substitution of deuterium will not significantly change their position.

2.4 The determination of the local magnetic fields at a Cl^{35} nucleus.

The magnitude of the local magnetic field at a Cl^{35} nucleus is given by the expressions we derived earlier.

$$B^2 = \left(\frac{2\pi}{\gamma}\right)\frac{1}{5}\{\Gamma_2 - \nu_{Qo}^2(1+\frac{\eta^2}{3})\} \qquad \text{(I-19)}$$

$$\Gamma_2 = \frac{1}{(2I+1)^2}\sum_{n=o}^{2I}\sum_{i=1}^{2I}\sum_{j=1}^{2I} c_i(n)c_j(n)\nu_i\nu_j . \qquad \text{(I-20)}$$

Thus the local field can be expressed in observables such as the absorption frequencies ν_i and the pure quadrupole frequency $\nu_Q = \nu_{Qo}(1+\frac{\eta^2}{3})^{\frac{1}{2}}$. Provided that these quantities can be obtained experimentally and the frequencies can be labeled ν_1, ν_2 and ν_3, which is essential for the calculation of Γ_2 , B can be found exactly.
The direction of the local field at a Cl^{35} nucleus can be found from

$$\vec{\nabla}_B\Gamma_2 = 5\left(\frac{\gamma}{2\pi}\right)^2\vec{B}\cdot\{\vec{\nabla}_B\vec{B}_1 + (\vec{\nabla}_B\vec{B}_1)_t\} \qquad \text{(I-24)}$$

$$\vec{\nabla}_B\Gamma_2 = \sum_{n=o}^{2I}\sum_{i=1}^{2I}\sum_{j=1}^{2I} c_i(n)c_j(n)\,\nu_1\vec{\nabla}_B\nu_j . \qquad \text{(I-22)}$$

$\vec{\nabla}_B\nu_j$ represents the direction in which a field should be applied to observe a maximum splitting of ν_j in the antiferromagnetic state. The direction of $\vec{\nabla}_B\Gamma_2$ belonging to one Cl^{35} position can then be found from (I-22) , provided again that we know how to label the observed frequencies ν_j. From (I-24) we see that the direction of $\vec{\nabla}_B\Gamma_2$ will in general not coincide with the local field $\vec{B}$.
As we mentioned before, the tensor relating these two directions may be called the field shift tensor. It contains elements of the symmetrized products of the dipole field tensor, the hyperfine tensor and the susceptibility tensor. The determination of the internal magnetic field direction with the aid of an external field (which may be a modulation

field or a constant field) requires complete knowledge of the principal axes and the principal values of these tensors, or at least of their symmetrized products. However, the determination of these values requires elaborate experiments on the splitting of the pure quadrupole lines of the Cl^{35} in the paramagnetic state. The sensitivity of the equipment and the small signal to noise ratio of the observed pure quadrupole resonances of the substances studied in this thesis did not permit such experiments. In general, however, the magnitude of the field shift tensor is rather small. The modified expression

$$\vec{\nabla}_B \Gamma_2 = 10\left(\frac{\gamma}{2\pi}\right)^2 \vec{B} \qquad \text{(II-3)}$$

will be a reasonable approximation[13].

The problem of finding the field at a Cl^{35} nucleus thus reduces to the selection of ν_1, ν_2 and ν_3 from the observed ν_i, ν_j and ν_k. This labeling problem can be complicated if we are dealing with more than one non-equivalent Cl^{35} nuclear site. In this case the number of observed frequencies is a multiple of three and our selection has to start with a search for the sets belonging to one particular nuclear site. Because the energy levels may be reversed, Γ_2 is unaltered by an interchange of ν_1 and ν_3, so only the assignment of ν_2 is unique. From computer solutions it can be shown that ν_2 can never be assigned to the highest observed frequency so the selection problem reduces to two possibilities. In the following part we will enumerate some criteria through which we possibly can decide what possibility should be taken.

a) Γ_2

The local magnetic fields at a ligand ion as Cl^{35} and a proton of the water of hydration are both a summation of hyperfine and dipolar fields. These two types of magnetic interaction are both proportional to the expectation value of the magnetic moment on the transition metal ion. Concluding we may say that the local fields at a Cl^{35} nucleus will be proportional to the local field at a hydrogen atom in the water of hydration. Thus if we plot for a series of temperatures $\Gamma_2(T)$ versus $\nu^2_{proton}(T)$, we will obtain a straight line according to (I-19). Extrapolation to $\nu^2_{proton}(T)$ is zero gives a value for $\nu_Q = \nu_{Qo}(1+\frac{\eta^2}{3})^{\frac{1}{2}}$. Whether this value agrees with the experimentally observed pure quadrupole frequency depends on the fact whether the energy level scheme we composed by labeling the observed frequencies applies to

the case. If the labeling is not correct, we are in fact calculating the second moment of an imaginary energy level scheme which will not be compatible with the observed pure quadrupole frequency.
However, it should be mentioned that even a correct selection does not always yield a value of ν_Q close to the observed paramagnetic ν_Q. The reason for this may be sought in the rather long extrapolation because usually data points close to T_N are not available, or in the fact that we do assume that ν_Q in the paramagnetic state is the same as in the antiferromagnetic state, which may not be true.

b) Γ_3

For nuclei with I=3/2 the third moment Γ_3 can be written as

$$\Gamma_3 = \nu_{Qo}\nu_Z^2 \{3\cos^2\theta - 1 + \eta \sin^2\theta\cos 2\phi\} \qquad \text{(I-19)}$$

and expressed in the frequencies ν_1, ν_2 and ν_3 from (I-21)

$$\Gamma_3 = \frac{3}{8}\{(\nu_1 + 2\nu_2 + \nu_3)(\nu_3^2 - \nu_1^2)\} . \qquad \text{(II-4)}$$

Applying the same argument as above we see that a plot of Γ_3 versus $\nu^2_{proton}(T)$ will yield a straight line through the origin, provided the labeling of the frequencies is correct. This offers a second check on the labeling.

c) Cl^{37}

The natural abundance of the Cl^{37} isotope is 25% . In general they show a set of absorption lines similar to those arising from the Cl^{35} nuclei, at a somewhat lower frequency and with a signal to noise ratio of approximately one fourth of the Cl^{35} lines. Both the gyro-magnetic ratio γ and the quadrupole moment Q of a Cl^{37} differ from those of a Cl^{35} nucleus. The ratio $\gamma^{35}/\gamma^{37} = 1.202$ and $Q^{35}/Q^{37} = 1.27$. One may calculate the ratio ν_i^{35}/ν_i^{37} of the corresponding transitions in the two sets and compare these values with those predicted by the second order perturbation theory formulas derived in chapter I.
From (I-9) we find,

$$\begin{aligned} \nu_1 &= \nu_Z - A\nu_{Qo} + B\nu_{Qo}^2/\nu_Z \\ \nu_2 &= \nu_Z \qquad - B\nu_{Qo}^2/\nu_Z + C\nu_{Qo}^2/\nu_Z \\ \nu_3 &= \nu_Z + A\nu_{Qo} + B\nu_{Qo}^2/\nu_Z \ , \end{aligned} \qquad \text{(II-5)}$$

where

$$A = \tfrac{1}{2}\{3\cos^2\theta - 1 + \eta \sin^2\theta\cos2\phi\}$$

$$B = \tfrac{3}{2}\sin^2\theta\{\cos^2\theta(1 - \tfrac{2}{3}\eta\cos2\phi) + \tfrac{1}{9}\eta^2(1 - \sin^2\theta\cos^2 2\phi)\}$$

$$C = \tfrac{3}{16}\{\sin^4\theta + \tfrac{2}{3}\eta \sin^2\theta(1 + \cos^2\theta)\cos2\phi + \tfrac{1}{9}\eta^2(4\cos^2\theta + \sin^4\theta\cos^2 2\phi\} . \qquad \text{(II-6)}$$

With (II-5) , the above mentioned ratios of γ and Q and $\nu_{Qo}/\nu_Z = Y < 1$ we can derive,

$$\begin{aligned} \nu_1^{35}/\nu_1^{37} &= 1.202 - Y(0.07A) + Y^2(0.14B - 0.07A^2) + \ldots \\ \nu_2^{35}/\nu_2^{37} &= 1.202 \qquad\qquad + Y^2(0.14C - 0.14B) + \ldots \\ \nu_3^{35}/\nu_3^{37} &= 1.202 + Y(0.07A) + Y^2(0.14B - 0.07A^2) + \ldots \end{aligned} \qquad \text{(II-7)}$$

From (II-6) and (II-7) one may show by numerical calculation that, in this approximation, with $Y < \frac{1}{2}$ and $\eta\cos2\phi < +0.3$, one of the three ratios will lie on the other side of 1.202 as the remaining two for all θ. Beyond this limit there is a small θ range where this condition is not fullfilled. This criterion may be used in sampling the lines belonging to one set when one deals with more than one inequivalent chlorine site. For the labeling within a set of three lines the fact that $|\nu_2^{35}/\nu_2^{37} - 1.202| < 5.10^{-2}Y^2$, can be useful.

d) Gradients.

The experimentally determined gradients of the Cl^{35} frequencies (see section 1.6) contain information which can be used in our selection. We did not succeed in extracting general rules from this information but nevertheless there exist some tendencies which can be useful.

When η is zero, the gradients of the lines in one set will lie in the plane through $\vec{B}$ and the principal z axis, as can be shown by applying $\vec{\nabla}_B = \vec{\xi}\frac{\partial}{\partial B} + \vec{\theta}\frac{1}{B}\frac{\partial}{\partial\theta} + \frac{\vec{\phi}}{B\sin\theta}\frac{\partial}{\partial\phi}$ to the relevant expressions for ν_i(II-5). Numerical calculations on the θ components for $Y \leq \frac{1}{2}$ of these gradients show that the $\vec{\nabla}\nu_1$ and $\vec{\nabla}\nu_2$ will be spread around $\vec{B}$ while $\vec{\nabla}\nu_2$ will lie between them for all θ values. It does not seem to be generally true that $\vec{\nabla}\nu_2$ will lie close to the gradient of the high frequency line as was suggested by Spence[13]. In the case when η is zero e.g. this condition is not fullfilled for θ values between 45 and 55 degrees.

In the case where η is not zero and $|\eta\cos 2\phi|$ is not too large, the gradients of ν_1 and ν_3 will move out of the original plane because of the ϕ dependence of the gradients. However, because the ϕ components are about equal in magnitude but have opposite signs and the influence of ϕ on the gradient of ν_2 is small, the three gradients will still be approximately coplanar. The aforementioned criterion that $\vec{\nabla}\nu_2$ will lie between the two others will still hold in a considerable range of values of $|\eta\cos 2\phi|$. A consequence of the small θ and ϕ dependence of the $\vec{\nabla}\nu_2$ is that its magnitude will be smaller than $|\vec{\nabla}\nu_1|$ and $|\vec{\nabla}\nu_3|$ except in those cases where all three are small. This will occur for θ angles close to 0° and 90°.

When the small field $\vec{\delta B}$ is a modulation field then $\delta B = \delta B_o \cos\omega t$ and the expressions are modified to:

$$A(\nu)_{tot} = 2A(\nu) + \frac{\partial^2 A(\nu)}{\partial \nu^2}(\vec{\nabla}_B \nu . \vec{\delta B}_o)^2 + \cos 2\omega t \frac{\partial^2 A}{\partial \nu^2}(\vec{\nabla}_B \nu . \vec{\delta B}_o)^2$$

This expression shows that the amplitude of the second harmonic will be zero if the direction of the modulation field is perpendicular to $\vec{\nabla}_B \nu$. The intensity measurement using second harmonic detection thus provides a convenient way to determine the direction of $\vec{\nabla}_B \nu$. However, if the symmetry of the aspect group is high, i.e. when we are dealing with a number of symmetry related $\vec{\nabla}_B \nu$ all belonging to one particular ν_i, the minima will overlap and we are forced to do the much more elaborate splitting experiments described in the first part of this section.

2.5 The determination of $\vec{\nabla}_B \nu_i$

As we showed in one of the previous sections, the determination of the local field direction at a nuclear site requires the knowledge of the gradient of ν_i with respect to $\vec{B}$. In general this direction can be found in two ways which are essentially the same.

The first method consists of measuring the splitting of a particular zero field absorption line as a function of the direction of a small applied d.c. field. The splitting of such a line will in general yield a number of absorption pairs. The pairs do originate from the inversion related fields and they will be about equally displaced with respect to the original zero field frequency. The number of pairs will depend on the number of elements in the aspect group of the crystal. The gradient, $\vec{\nabla}_B \nu_i$ will coincide with the direction in which the external field should be applied to observe a maximum splitting within a pair. The maximum splitting direction of other pairs will be symmetry related to the former one. The magnitude of $\vec{\nabla}_B \nu_i$ can be obtained by dividing the observed maximum splitting $\Delta\nu_i$ by twice the magnitude of the applied magnetic field.

The second method is based on intensity measurements of the unsplit absorption line as a function of the orientation of an a.c. modulation field. A small field $\delta\vec{B}$ will split the absorption line in sets of two components. We will consider only one set here, the effect of the others can be found by summation. Let the zero field absorption curve be represented by $A(\nu)$. A small external field $\delta\vec{B}$ will cause a simultaneous shift $\delta\nu$ of the absorption curve in the plus and minus direction of the frequency axis. So at any moment the total absorption at a frequency ν with an external field $\delta\vec{B}$ causing a shift $\delta\nu$ of each of the two components can be written as:

$$
\begin{aligned}
A(\nu)_{tot} &= A(\nu + \delta\nu) + A(\nu - \delta\nu) \\
&= A(\nu) + \frac{\partial A}{\partial \nu}\,\delta\nu + \tfrac{1}{2}\,\frac{\partial^2 A}{\partial \nu^2}\,\delta\nu^2 + \text{-----} \\
&\quad + A(\nu) - \frac{\partial A}{\partial \nu}\,\delta\nu + \tfrac{1}{2}\,\frac{\partial^2 A}{\partial \nu^2}\,\delta\nu^2 + \text{-----} \\
&= 2A(\nu) + \frac{\partial^2 A}{\partial \nu^2}\,\delta\nu^2
\end{aligned}
$$

and since $\delta\nu = \vec{\nabla}_B \nu \,.\, \delta\vec{B}$, we may write

$$
A(\nu)_{tot} = 2A(\nu) + \frac{\partial^2 A(\nu)}{\partial \nu^2}\,(\vec{\nabla}_B \nu .\, \delta\vec{B})^2 \,.
$$

CHAPTER III

EXPERIMENTAL APPARATUS

3.1 Introduction .

In this chapter we will briefly review the experimental set up as used in our experiments.

3.2 Apparatus.

The N.M.R.data were taken on a conventional marginal oscillator spectrometer, described elsewhere in literature[18]. Large signals could be displayed directly on the oscilloscope, small signals were detected by synchronous first or second harmonic detection. The modulation field was provided by a pair of Helmholtz coils placed outside the cryostat, which could be rotated about a vertical axis; the modulation frequency was 290 Hz. The samples were mounted on a goniometer (figure III-1). The goniometer allowed a 360° rotation of the crystal around a fixed horizontal axis during the experiments. It consisted of a plastic disc mounted with a stainless steel axel in a frame of the same material. The disc could be rotated by means of a string wound twice around its circumference with one end attached by a spring to a brass plate on top of the cryostat; the other end of the string could be moved up and down using a simple screw mechanism on top of the cryostat.

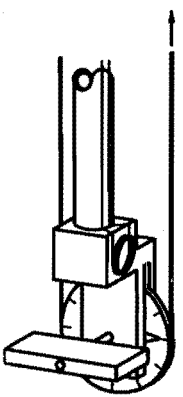

Fig.III-1
The goniometer.

The position of the rotation axis with respect to the modulation field could be found by monitoring the induced voltage of the modulation field in a small flat pick-up coil attached to one of the vertical sides of the goniometer. In this way an accuracy of about 0.2 degrees could be obtained. The temperature of the He^4 bath was measured by its vapour pressure. The temperatures from $4.2^{\circ}K$ to $5.0^{\circ}K$ were obtained by allowing the pressure inside the cryostat to build up to a maximum of 150 cmHg.

CHAPTER IV

METHOD FOR THE DETERMINATION OF ASYMMETRIC CRYSTALLINE ELECTRIC-FIELD-GRADIENT TENSORS WITH APPLICATION TO $Cs_2MnCl_4.2H_2O$.[19]

4.1 Introduction

In this chapter, a relatively simple, experimentally convenient procedure is described for the determination, from nuclear magnetic-dipole-electric quadrupole resonance data, of the asymmetry parameter of the electric field gradient tensor and of its orientation relative to the crystal, provided that the externally applied magnetic field is sufficiently large to make the magnetic dipole interaction appreciable stronger than the electric quadrupole interaction. The relevant theoretical considerations are given in section 4.2. Experimental procedures and specific application to the ^{133}Cs resonance in $Cs_2MnCl_4.2H_2O$ are discussed subsequently.

4.2 Theory

The Hamiltonian for the interaction of a nucleus of magnetic dipole moment $\vec{\mu}$ and electric quadrupole moment tensor $\overleftrightarrow{Q}$ with a magnetic field $\vec{B}$ and an electric field gradient $\overrightarrow{\nabla E}$ on a coordinate system which diagonalizes the Zeeman interaction was derived in chapter I. Although the case I = 3/2 was emphasized, the general expressions are valid for any value of I. Perturbation calculations in the high-field case showed that (II-9):

$$E_m^o = -\nu_Z m, \qquad m = I, I-1, \cdots, -I \qquad \text{(IV-1)}$$

and the first-order perturbation energies are given by

$$E_m^1 = \frac{\nu_{Qo}}{4}\{m^2 - I(I+1)\}(3\cos^2\theta - 1 + \eta\sin^2\theta\cos 2\phi). \qquad \text{(IV-2)}$$

From this, it is seen that the first-order shifts E_m^1 vanish if the applied magnetic field is oriented with respect to the field gradient tensor in such a way that

$$3\cos^2\theta - 1 + \eta\sin^2\theta\cos 2\phi = 0 \ , \qquad \text{(IV-3)}$$

or equivalent , that

$$\sin^2\theta = \frac{2}{3(1 - \frac{1}{3}\eta\cos 2\phi)} \ . \qquad \text{(IV-4)}$$

For these orientations, the frequency pattern observed is thus, to the first order of approximation, a pure Zeeman pattern, i.e., all $\Delta m = \pm 1$ transitions coalesce at a single frequency which is equal to the Zeeman frequency one would observe in the absence of quadrupole interaction. The second-order contributions to the energy E_m^2 (I-9) show that

$$E_m^2 = - E_{-m}^2 \ . \qquad \text{(IV-5)}$$

Thus for any direction of the applied field the orientations specified by the $\Delta m = \pm 1$ transition frequencies coalesce in pairs, except for the $\frac{1}{2} \rightarrow - \frac{1}{2}$ transition (in case of half-integral spin) which is unique. The pairwise coalescence of the transition frequencies, moreover, occurs with the entire frequency pattern showing minimum over-all splitting. The CRO display of such frequency patterns allows easy identification of the directions (θ,ϕ) for which (IV-4) is satisfied. The locus of all such directions (θ,ϕ) is a cone whose axis is the z axis of the electric field gradient tensor and whose intersections with planes perpendicular to the z axis are elliptical. The ratio of the minor to the major axis of the elliptical cross sections is $(1 - \eta)/(1 + \eta)$, the apex angle of the cone is 2θ. For $\eta = 0$, the cone is a right circular one, while the apex angle is constant and equal to 109.4°.
Now, from (IV-4) one has that

$$\sin^2\theta_{max} = \frac{2}{3(1 - \frac{1}{3}\eta)} \ , \text{ when } \phi = 0^\circ \text{ and } \phi = 180^\circ \qquad \text{(IV-6)}$$

and

$$\sin^2\theta_{min} = \frac{2}{3(1 + \frac{1}{3}\eta)} \ , \text{ when } \phi = 90^\circ \text{ and } \phi = 270^\circ. \qquad \text{(IV-7)}$$

The major and minor directions of the elliptical cross sections can thus be inferred from experiment. The principal axes of the electric field gradient tensor are thereby determined in a relatively easy way, and η can be determined from (IV-6) or (IV-7).

It can be seen from (IV-1) and (IV-5) that the sum of the cubes of the (2I + 1) eigen values E_m,

$$\Gamma_3 = \sum_m (E_m)^3 \qquad \text{(IV-8)}$$

is equal to zero through the second order of approximation when (IV-4) holds. Brown and Parker[9] showed that the exact, general value of Γ_3 is given by

$$\Gamma_3 = p_3 \nu_{Qo}^3 (1 - \eta^2) + 3p_2 \nu_{Qo} \nu_Z^2 (3\cos^2\theta - 1 + \eta \sin^2\theta \cos 2\phi) \qquad \text{(IV-9)}$$

where p_2 and p_3 are certain polynomials in I. This reduces to

$$\Gamma_3 = p_3 \nu_{Qo}^3 (1 - \eta^2) \qquad \text{(IV-10)}$$

when (IV-4) is satisfied. The angle-independent contribution to Γ_3 must therefore be solely due to effects of orders higher than the second. It is zero for $I = \frac{3}{2}$ (for which $p_3 = 0$), and it is zero for all I when $\eta = 1$. For these special cases, the "minimum splitting" situation described above is exact, and for more general situations it is approximate to second order in energy.

4.3 Experimental

To trace out experimentally the elliptical cone of minimum splitting one requires an apparatus in which all orientations of the applied magnetic field with respect to the crystal are accessible. In our experiment, this was done by mounting the crystal on a goniometer which allowed for a rotation ω of the crystal around an axis Ω perpendicular to the rotation axis Φ of the magnetic field. Thus, with respect to the crystal, a complete rotation ω corresponds to a rotation of Φ around Ω. These remarks are illustrated in figure IV-1. If Ω lies within the cone of minimum splitting, then for a given ω, four magnetic field positions of minimum splitting can be identified. These directions (ϕ_1, ϕ_2, $\phi_1 + 180^\circ$, $\phi_2 + 180^\circ$) mark the intersection of the elliptical cone with the plane of rotation of the magnetic field. If Ω lies outside the cone then there are no angles ω for which obvious minimum splitting can be observed. The set of minimum splitting data $\phi(\omega)$ is plotted on a stereographic net with the projection of the Ω axis in the pole. The resulting figure represents a

cross section of the elliptical cone with a spherical surface and has twofold symmetry around the z-axis. In general, however, this symmetry is not easily recognized unless the figure is rotated until the z-axis is in the pole of the projection. In that case, the twofold symmetry is readily apparent, as can be seen from figure IV-2. Magnitude and direction of the required rotation are found by trial and error. The position of the electric field gradient tensor with respect to the crystal, at the inversion center of the figure, can be found by shifting the entire figure back to its original position. The conical axes Θ_{max} and Θ_{min} can be obtained from the major and minor axes of the locus.

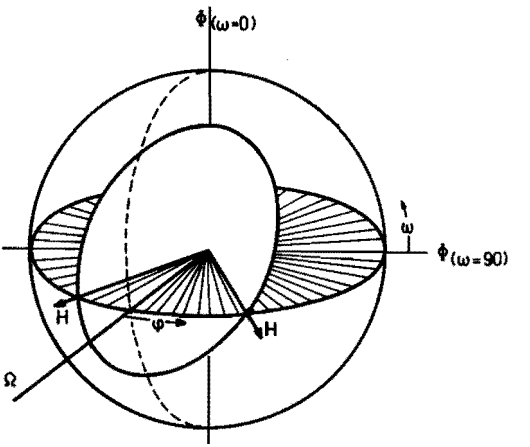

Fig.IV-1 Relative positions of the rotation axes and the elliptical cone of minimum splitting in a general case.

4.4 Application to $Cs_2MnCl_4.2H_2O$.

The techniques described in the previous sections were used to determine the electric field gradient tensor at the Cs sites of $Cs_2MnCl_4.2H_2O$. This crystal is one of a series of Mn compounds in which NMR signals have been observed recently [13,20]. The crystal structure as determined by Jensen[21] is triclinic and there is one chemical formula unit per unit cell. The ^{133}Cs nucleus has a spin of $I = \frac{7}{2}$ and a quadrupole moment, as listed by Varian, of $-0.004 \times 10^{-24} cm^2$, giving rise to maximum splittings of the order of 100 kc/sec in applied fields of several thousand gauss. Thus the quadrupole interaction can be regarded as small compared to the Zeeman interaction, and our technique can be

applied. The experiment was performed at liquid-nitrogen temperatures on single crystals grown from an aqueous solution.
The experimental results together with the rotated projection are shown in figure IV-2 from which the directions of the major and minor axes of the electric field gradient tensor can be found. The orientation with respect to the crystal axes is given in figure IV-3. The asymmetry parameter can be calculated from (IV-6) and (IV-7). Using the experimental values $\Theta_{max} = 82.8 \pm 0.5^{\circ}$ and $\Theta_{min} = 46.6 \pm 0.5^{\circ}$, we find

$$\eta = 0.81 \pm 0.01$$

from (IV-6), and

$$\eta = 0.79 \pm 0.06$$

from (IV-7) it appears that the value of η calculated from Θ_{min} is much more sensitive to small errors in angle than the value of η calculated from Θ_{max}. Therefore, we quote as our result that

$$\eta = 0.81 \pm 0.01$$

This result may be compared with $\eta = 0.78$ at the Rb sites in $Rb_2MnCl_4.2H_2O$ where η can be calculated from the pure quadrupole resonance data of the two available Rb isotopes[13].

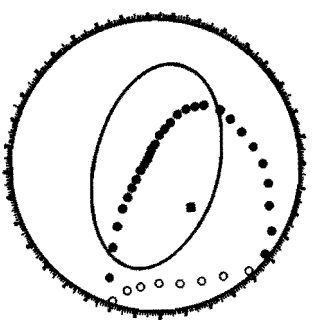

Fig.IV-2 The set of data points on the elliptical cone in stereographic projection. The solid curve represents the same projection rotated such that its twofold symmetry is apparent. The square datum point gives the direction of the electric field gradient axis.

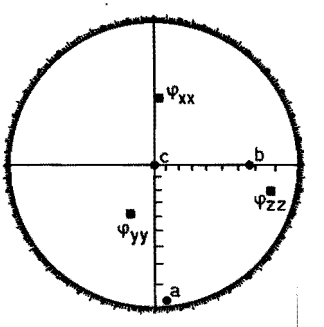

Fig.IV-3 The axes of the electric field gradient tensor at the Cs sites in $Cs_2MnCl_4.2H_2O$ with respect to the crystal axes. Solid data points are upperhemisphere projections and the open data points are lowerhemisphere projections.

CHAPTER V

NUCLEAR MAGNETIC RESONANCE IN $CsMnCl_3.2H_2O$[22].

5.1 Introduction

The complex hydrated manganese chlorides present a wide variety of crystal structures. Consequently they offer an excellent opportunity to explore the relation between crystal structure and magnetic ordening. $CsMnCl_3.2H_2O$ is a particularly interesting member of this set of compounds in that susceptibility[23] and specific heat studies[24] indicate that a great deal of ordening occurs at temperatures well above the antiferromagnetic ordening temperature of 4.89^oK. In both cases the experimental results can be explained quite accurately by assuming the existence of antiferromagnetic linear chains at temperatures above the three dimensional ordening temperature.

The present chapter is concerned primarily with determining the magnetic structure of the antiferromagnetic phase found below 4.89^oK. Nuclear magnetic resonance data from the Cl, Cs and H nuclei together with the direction of sublattice magnetization determined from magnetic susceptibility measurements and zero field spin flopping, serve to completely determine the magnetic space group.

In section 5.2 and 5.3 we will briefly review the crystallography of the compound, the preparation of the samples and the quality of the signals. Sections 5.4 to 5.6 give an outline of the experimental N.M.R. results on the various nuclei. These results are then used to deduce the magnetic space group in section 5.7 .Section 5.8 concludes this chapter with some remarks about the exchange interactions.

5.2 Crystallography

The existence of the salt $CsMnCl_3.2H_2O$ was reported by Saunders[25] who concluded the structure to be orthorhombic. An x-ray structure determination was published recently by Jensen[26] et al. The crystallographic space group appears to be P_{cca} with 4 formula units in a chemical unit cell. In table V-1 the atomic parameters and lattice constants are summarized.

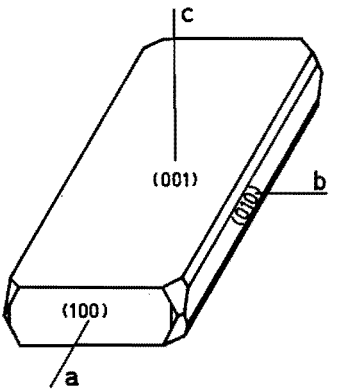

Fig.V-1 Usual morphology of $CsMnCl_3 \cdot 2H_2O$ showing the axes used in this chapter.

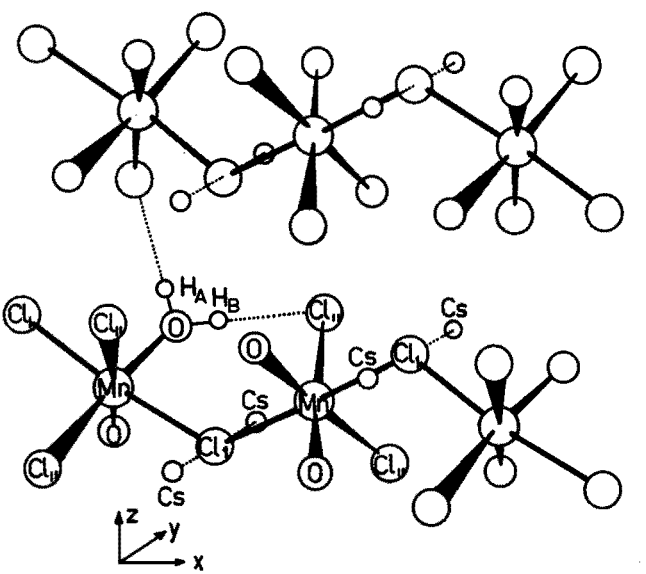

Fig.V-2 Structure of $CsMnCl_3 \cdot 2H_2O$ according to Jensen et.al. Only one set of hydrogens and hydrogen bonds are shown.

Table V-1. Room temperature lattice parameters and atomic coordinates in $CsMnCl_3.2H_2O$.

P_{cca} : position	a = 9.060 a	b = 7.285 b	c = 11.455 c
Cs	0.250	0.000	0.146
Mn	0.000	0.467	0.250
Cl_I	0.250	0.500	0.146
Cl_{II}	0.085	0.228	0.391
O	0.080	0.669	0.361
H_I	0.031	0.699	0.434
H_{II}	0.183	0.701	0.370

The shape of the crystals, which grow very easily by evaporation of a saturated equimolar solution of CsCl and $MnCl_2.4H_2O$ in water, is drawn in figure V-1. The (001) plane is always recognized at once because, apart from the fact that it is the largest face, the crystal cleaves very easily parallel to this plane. Without using x-rays to distinguish between the {100} and {010} direction, confusion between these may occur because the interfacial angles are almost equal .

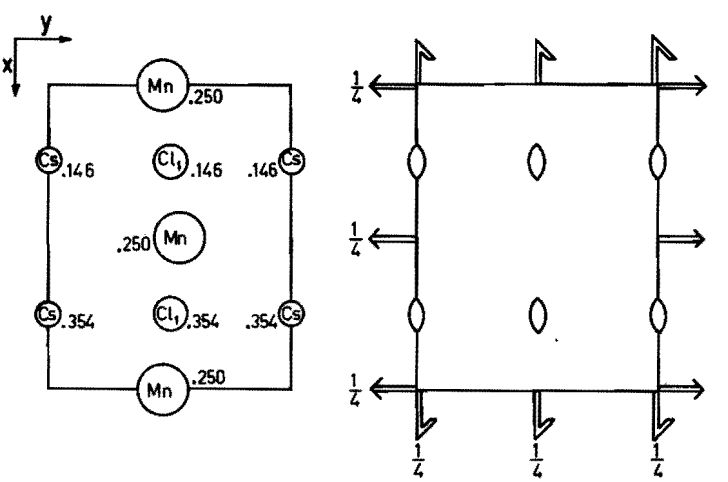

Fig. V-3 Space group P_{cca} of $CsMnCl_3.2H_2O$ showing, on the left side, the special positions of the Mn, Cs and Cl_I nuclei.

The structure consists of octahedra of four chlorine and two oxygen atoms . These octahedra share one chlorine atom thus forming a chain along the a axis (figure V-2). The chains are separated in the b direction by layers of Cs atoms. The Mn, Cs and one of the Cl atoms, which we will call Cl_I, occupy special positions on two fold axes. (figure V-3).

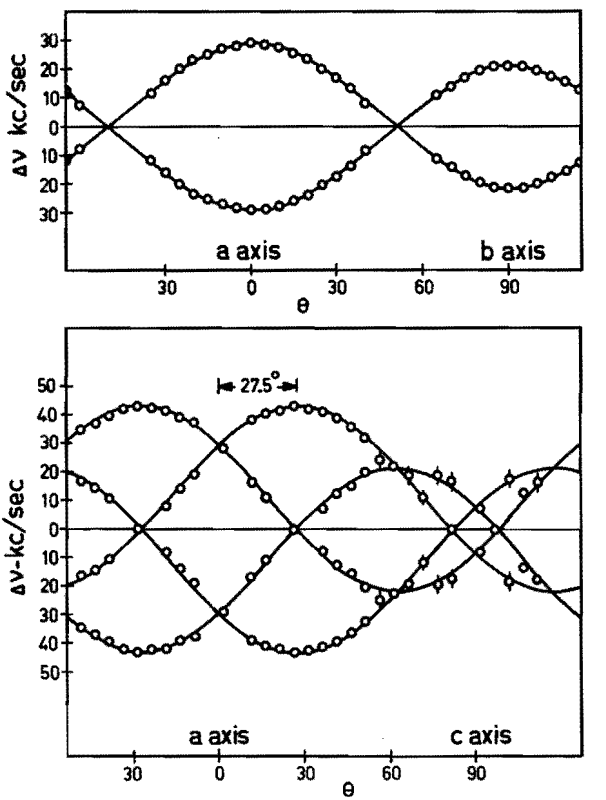

Fig.V-4 Dipole-dipole splitting of the protons in $CsMnCl_3.2H_2O$ at room temperature in an external field of 1350 Oe. The drawn curves represent the calculated angular dependence on the basis of the assumed hydrogen bonds and proton positions.

The proton positions were taken as lying on the two shortest O--Cl bonds, at a distance of 0.987Å from the oxygen as suggested by El-Saffar[27]. The validity of this hydrogen bonding scheme and the proton positions were checked experimentally by applying the techniques we discussed in section

2.3. First it was shown that this hydrogen bonding scheme predicts correctly the magnitude and the angle dependence of the proton nuclear dipole-dipole line splitting observed at room temperature. The results of these experiments are shown in figure V-4. The drawn curve represents the expected angle dependence on the basis of the hydrogen bonding scheme and the well known formulas for the dipole-dipole splitting (II-1). As can be seen from figure V-4, the data points coincide almost exactly with the calculated curve. Secondly, the electric field gradient tensor at the deuterium nuclei in $CsMnCl_3.2D_2O$ was determined. The results are plotted in stereogram V-5. As one can see, the principal z axes lie within a few degrees of the O---H directions; therefore we may conclude that our assumed hydrogen positions are approximately correct.

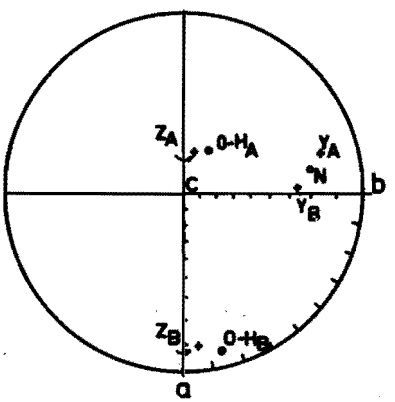

Fig.V-5 Stereographic projection of two principal axes (Z,Y) of the electric field gradient tensor on the deuterium nuclei (A,B) belonging to one water molecule in $CsMnCl_3.2D_2O$. O-H_A, O-H_B and N represent respectively the two oxygen-proton vectors in a water molecule and the vector perpendicular to the H_A-O-H_B plane. Only one of the symmetry related sets is shown.

The hydrogen bond establishes a weak bond between the layers parallel to the a-b planes. This is probably the explanation of the existence of a cleavage plane perpendicular to the c axis.

5.3 Preparation and detection.

Crystal specimens used in the experiments were grown by evaporation at room temperature from a solution of $MnCl_2.4H_2O$ and CsCl in water and were ground into spheres with a radius of about 3 mm. The spheres were oriented in the goniometer, described in chapter III, using x-rays. After the experiments the orientation was checked again. Most of the experiments were performed on one sample. The entire goniometer and the crystal were immersed in liquid He during the experiments. Temperatures in the range from 4.2 - 1.1°K were obtained by pumping the helium, temperatures from 4.2 - 5.0°K were obtained by raising the pressure in the helium dewar up to 140 cmHg.
In general the signals were of lower intensity then those found in other complex manganese chlorides[13,20]. Good signal to noise ratios seemed to require the use of samples which were at least approximately spherical in shape.

5.4 Chlorine resonance.

a) Temperature dependence.
As previously shown in figure V-3 there are two distinct Cl sites in $CsMnCl_3.2H_2O$. The Cl_I sites link two Mn ions in the lineair chain.
If the chains are assumed to be antiferromagnetic the transfer hyperfine interactions from the two neighbouring Mn ions should cancel and the field at the Cl_I site would be expected to be small and largely dipolar in origin.
For the Cl_{II} sites the transfer hyperfine field from only one Mn ion should be operative. Results from other manganese chlorides[13,20] show that at such a site one expects, at temperatures well below the Néel temperature, to find a transfer hyperfine field of the order of 20 kOe combined with a much smaller dipolar field.
The temperature dependence of the Cl^{35} lines in the absence of an external field are shown in figure V-6. These results are precisely what one would expect on the basis of the conjectures mentioned above. The pairs of low frequency lines clearly belong to a site at which the internal magnetic field is so small that the Zeeman interaction is dominated by the quadrupole interaction. This results in the appearance of two α (the inner pair) and two β(the outer pair) transitions as was already shown in chapter I.

The α lines can be followed through the transition point at which they collapse into a single pure quadrupole line at a frequency of 6.16 Mc/sec. The Néel temperature resulting from such an experiment was found to be 4.889 ± 0.005°K. Following the reasoning of the preceding part we assign these pairs of lines to the Cl_I sites. The remaining three lines have a strong temperature dependence and must correspond to the $\Delta m = \pm 1$ transitions from the chlorines at the Cl_{II} sites. A second Cl^{35} pure quadrupole frequency found in the paramagnetic state at 4.184 Mc/sec. may be assigned to these chlorine atoms.
The Cl^{37} give a similar set of frequencies which do not contain essential new information and therefore will not be used.

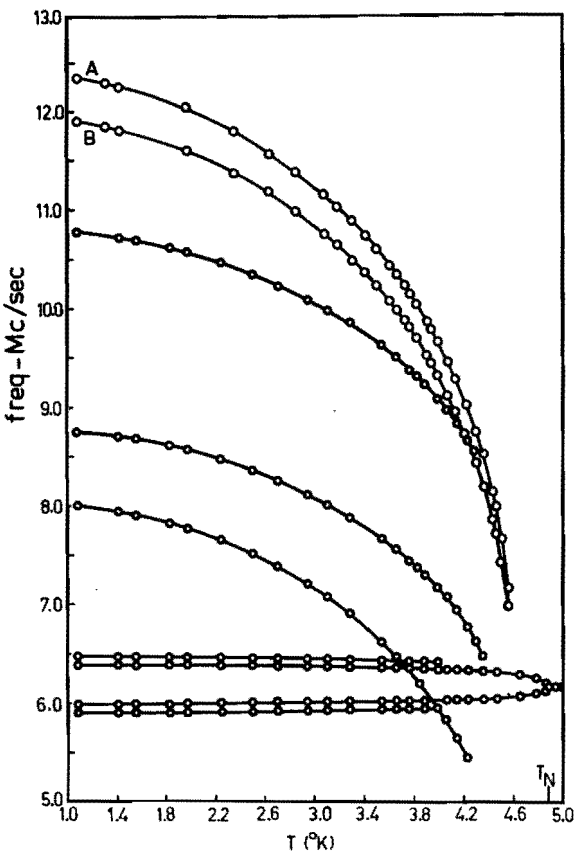

Fig.V-6 Temperature dependence of the Cl^{35} and the proton (A, B) lines.

b) Local magnetic fields at the chlorine nuclei.

As we saw in chapter II, the local field magnitude at a Cl nucleus can be found from

$$B^2 = \{ \frac{2\pi}{\gamma} \}^2 \frac{1}{5}\{\Gamma_2 - \nu_{Qo}^2\} \qquad \text{(I-19)}$$

and the direction of the local magnetic field from

$$\vec{\nabla}_B \Gamma_2 = 10\{ \frac{\gamma}{2\pi} \}^2 \vec{B} . \qquad \text{(II-3)}$$

Both expressions require the knowledge of Γ_2 and thus the labeling of the observed transition frequencies. We will apply this mathematical technique only to the set of frequencies arising from the Cl_{II} site, because the local fields at the Cl_I sites can be found in a much simpler way.
The selection criteria summarized in section 2.4 will be used in order to find the correct labeling of the Cl_{II} transition frequencies.
The results, for the two possibilities of labeling, of the extrapolation of Γ_2 and Γ_3 versus ν^2_{proton} plots are summarized in table V-2.

Table V-2 Summary of some parameter values used in the labeling procedure. Frequencies are given in Mc/sec.

ν_i *	label**	$\frac{2\pi}{\gamma}\lvert\vec{\nabla}_B\nu\rvert$	exp.ν_Q	extrapolation Γ_2	extrapolation Γ_3
7.156	ν_2	1.09			
8.078	ν_1	1.23	4.184	4.53	<10
10.058	ν_3	1.15			
7.156	ν_1	1.09			
8.078	ν_2	1.23	4.184	5.82	520
10.058	ν_3	1.15			

* at $\Gamma = 3.0^oK$

** ν_1 and ν_3 may be interchanged.

The conclusion from these criteria must be that the lowest frequency should be labeled ν_2. Applying a small external field one can determine the $\vec{\nabla}_B\nu_i$ from each of the three Cl_{II} frequencies. An example of one of

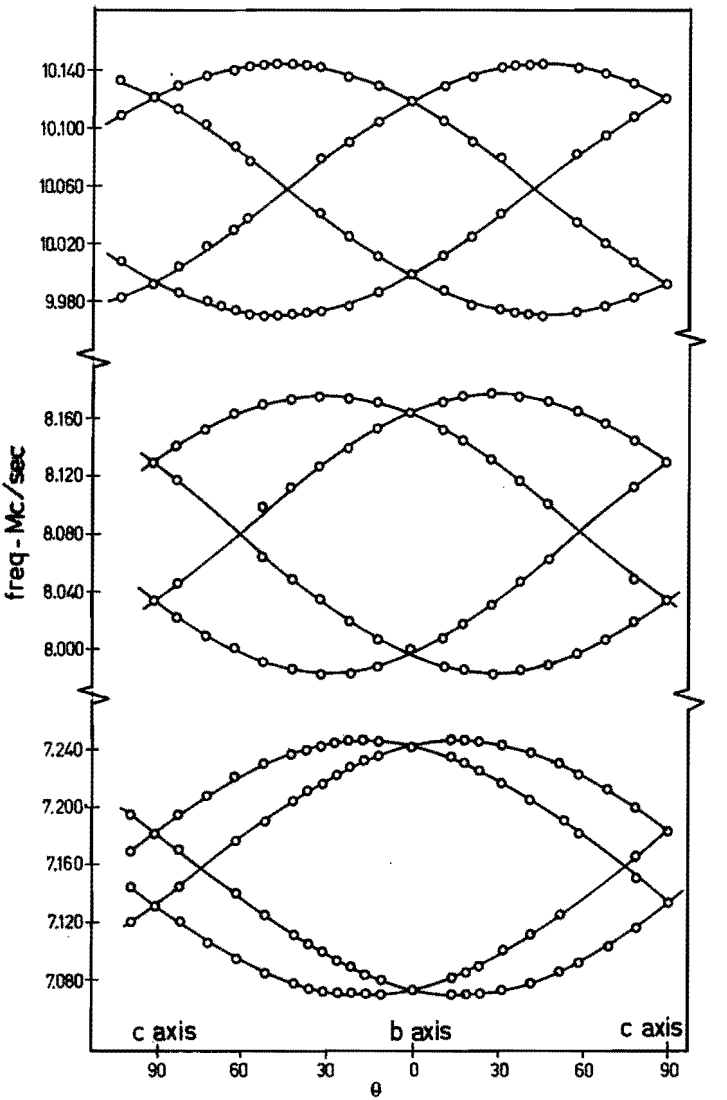

Fig.V-7 Angular dependence of the splitting of the Cl_{II} lines in an external field of 190 Oersted at T = 3.0 K.

those splitting experiments is shown in figure V-7. A combination of several of these rotation diagrams results in the $\vec{\nabla}_B \nu_i$ plotted in figure V-8 and tabulated in table V-2. In section 2.4 we have already mentioned that the $|+\frac{1}{2}) \leftrightarrows |-\frac{1}{2})$ transition, which we called ν_2, can in general be identified by the fact that the direction of $\vec{\nabla}_B \nu_2$ will lie between the

two others and its magnitude will be the smallest one. Selection of ν_2 based on this criterion agrees completely with the first one.
Having solved the labeling problem we can calculate the local fields with I-19 and II-3. For a chlorine nucleus with I = 3/2, (II-3) can be written with (I-22) as

$$\vec{B} = \{\frac{2\pi}{\gamma}\}^2 \frac{1}{40} \{ \vec{\nabla}_B\nu_1 (\tfrac{3}{4}\nu_1 + \tfrac{1}{2}\nu_2 + \tfrac{1}{4}\nu_3) + \\ + \vec{\nabla}_B\nu_2 (\tfrac{1}{2}\nu_1 + \nu_2 + \tfrac{1}{2}\nu_3) + \\ + \vec{\nabla}_B\nu_3 (\tfrac{1}{4}\nu_1 + \tfrac{1}{2}\nu_2 + \tfrac{3}{4}\nu_3) \} . \qquad \text{(V-3)}$$

Before we can add the gradients with their relative weight factors, we have to know which set of gradients $\vec{\nabla}_B\nu_i$ originates from one particular nuclear site. This problem can be solved when one realises that only when the correct combination of $\vec{\nabla}_B\nu_i$ is used , Γ_2 will yield the values $\Gamma_2(0) + (\gamma/2\pi)^2 B^2_{ext}$ when an external field $\vec{B}_{ext}$ is applied in the direction of $\vec{B}$ resulting from this particular combination. The magnetic fields at the Cl_{II} nucleus resulting from the ultimate selection are shown in stereogram V-9 and are tabulated in table V-3.

Table V-3 Internal fields for Cl_I, Cl_{II} and Cs nuclei.

nucleus	internal field-kOe at 1.8°K	orientations α	β	γ
Cl_I	0.68	90	90	0
Cl_{II}	20.88	84	14.5	77
Cs	2.32	66	24	90

Of course the same mathematical techniques may be applied to the Cl_I signals, with an adaption of the labeling to the α and β transitions. The fact, however, that the Cl_I nucleus lies on a twofold axis permits only two possible orientations for a non-zero magnetic field at that site, i.e. parallel or perpendicular to the twofold c axis. A single splitting experiment enables us to distinguish between these cases. The magnitude of the field follows immediately from the knowledge of the principal axes of the electric field gradient tensor, the determination of which we shall postpone till the next section. The results of the

measurements of the local field at the Cl_I nucleus are shown in figure V-9 and are tabulated in table V-3.

We see that the direction of the small field at the Cl_I site is directed along the c axis while the large fields at the Cl_{II} site cluster about the b axis. As former experiments [2,13] showed the transferred hyperfine interaction to be largely isotropic in ionic manganese compounds, it seemed rather unlikely that the a axis was the preferred direction of the Mn spins, as was reported by Smith e.a.[23]. A search for the zero frequency spin flopping yielded a value of 17.3 kOe. at 1.17°K when the magnetic field was applied along the b axis, thus indicating that the b axis was indeed the preferred direction. Susceptibility measurements by Cowen and Fairall[31] and Botterman and de Jonge[32] gave the same results.

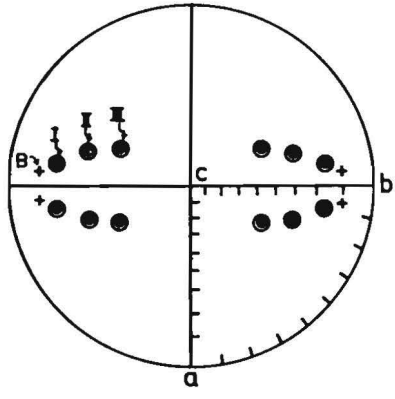

Fig.V-8 Stereographic projection of the $\vec{\nabla}_B \nu_i$ from the Cl_{II} transition at 3.0 K. I = 7.156 Mc/sec., II = 8,079 Mc/sec. and III = = 10.058 Mc/sec. The cross represents the ultimate local field direction at the Cl_{II} nuclei.

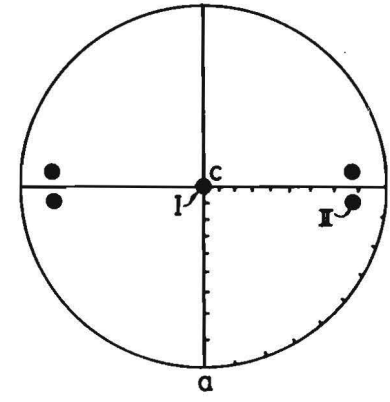

Fig.V-9 Stereogram of the local field directions at the two types of Cl^{35} sites.

Our chlorine resonance results can thus be interpretated as indicating that there is none or a vanishingly small isotropic transferred hyperfine field at the Cl_I sites, which will be confirmed by calculations of the dipolar field at the Cl_I site (section 5.7). For the Cl_{II} sites the directions and magnitudes of the internal field indicate that it arises

from a large isotropic transferred hyperfine interaction with smaller dipolar (and possibly anisotropic transfer) contributions.

c) Electric field gradient tensors at the Cl sites.
The principal axis of the E.F.G. tensor and the asymmetry parameter can be determined by comparing the angle dependence of the splitting of the pure quadrupole transition by a small external field, with the theoretical solutions discussed in chapter II.

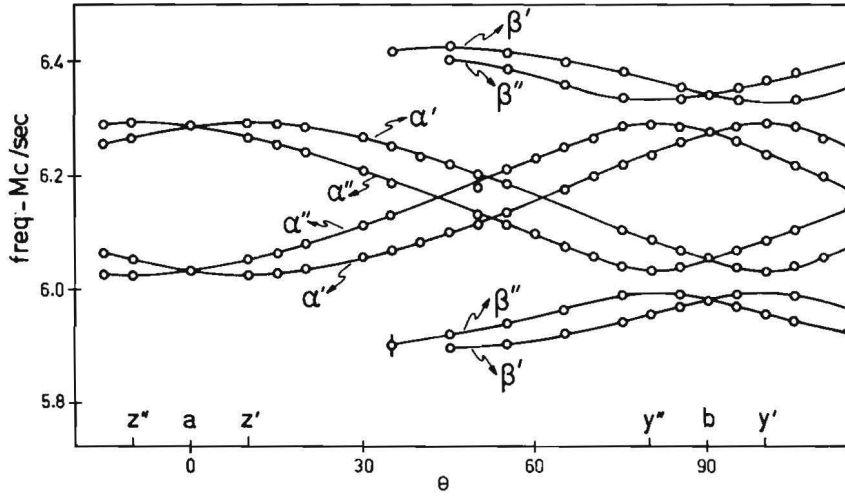

Fig.V-10 Angular dependence of the splitting of the Cl_I pure quadrupole transition in an external field of 314 Oersted at T=5.0 K.

The result of such a splitting experiment for the Cl_I nucleus is shown in figure V-10. The rotation plane of the magnetic field is perpendicular to the twofold c axis. Because of the special position of the Cl_I nucleus on that axis, symmetry requires that one of the principal axes from the E.F.G. tensor must coincide with the c axis, while the other two must lie in the a-b plane. Since the splitting of the α lines always shows a relative maximum when the magnetic field coincides with one of the principal axes of the E.F.G. tensor, we conclude that the two axes must lie at 10° from the a and b axis (figure V-10). The identification of the axes is possible by comparing the actually measured splittings of the α and β lines, when the magnetic field is directed along the axes, with

the transition frequencies following from the calculated energy levels in chapter I.
From (I-15) we find for I = 3/2 :

$$\Delta\nu_\alpha = 2\nu_Z \quad ; \quad \Delta\nu_\beta = 4\nu_Z/\rho \qquad \text{when B//Z}$$
$$\Delta\nu_\alpha = 2(1-\eta)\nu_Z/\rho \; ; \quad \Delta\nu_\beta = 2\nu_Z \qquad \text{when B//X} \quad (V\text{-}4)$$
$$\Delta\nu_\alpha = 2\nu_Z \quad ; \quad \Delta\nu_\beta = 2(1+\eta)\nu_Z/\rho \qquad \text{when B//Y}$$

where $\rho = (1 + \frac{\eta^2}{3})^{\frac{1}{2}}$ and $\nu_Z = \frac{\gamma}{2\pi} B$

Because the maximum splittings of the α lines in figure V-10 both have the same magnitude and differ significantly from the magnitude of the extrema of the β lines, we conclude that $\eta \neq 0$ and the two positions of maximum splitting have to be the Z and Y axis of the E.F.G. tensor. The position at 10^o from the a axis should thereby be assigned to the Z axis because figure V-10 clearly indicates that the splitting of the β lines will show a maximum there. The remaining X axis will consequently fall along the crystallographic c axis. In table V-4 the results are summarized.

Table V-4 Principal axes and asymmetry parameters at Cl_I, Cl_{II} and Cs Cs nuclei.

nucleus	axis	experimental				monopole model			
		orientation			asym.par.	orientation			asym.par.
		α	β	γ	η	α	β	γ	η
Cl_I	Z	10	80	90		15	75	90	
	Y	100	10	90	0.30±0.02	105	15	90	0.27
	X	90	90	0		90	90	0	
Cl_{II}	Z					74	49	46	
	Y					20	87	70	0.76
	X					80	42	50	
Cs	Z	43	48	90		46	43	90	
	Y	133	43	90	0.33±0.02	136	46	90	0.83
	X	90	90	0		90	90	0	

The asymmetry parameter η calculated from (V-4) is 0.31 ± 0.02 at $5^{o}K$. Once we know that the c axis coincides with the X axis of the E.F.G., we are able to calculate ν_Z and η from the data in the antiferromagnetic state. This results in $\eta = 0.29 \mp 0.02$ and a ν_Z as tabulated in table V-3.

Splitting experiments in the paramagnetic state at $14^{o}K$ and $5^{o}K$ on the Cl_{II} nucleus were not succesful . The signal to noise ratio appeared to be very poor because the general eight fold position of the Cl_{II} nucleus caused a splitting of the single pure quadrupole line in at least 8 components. However, we may approximate the θ and $\eta\cos 2\phi$ in the antiferro magnetic state by using the second order perturbation formulas (I-9) and the three measured transition frequencies. Such a calculation yields two θ values because the frequencies ν_1 and ν_3 can be interchanged. In this case θ can be 43^{o} and 55^{o}. The product $\eta\cos 2\phi$ will be -0.3 and -0.7 respectively. However, this number shouldn't be taken too seriously as it is very sensitive to small errors in θ. To distinguish between the two possibilities we carried out a computer calculation of the E.F.G. tensors in $CsMnCl_3.2H_2O$.

The calculation was based on a simple monopole model and the atomic contribution was considered to be small. The actual charge distribution was replaced by appropriate point charges on the atomic positions. The charge on the Cs, Mn and Cl positions were taken as + 1 , + 2 and - 1 respectively. The charge distribution within the water molecule was approximated by - 1 on the oxygen and + 0.5 on the hydrogen atoms. These values were taken as an average between the values based on the static electric dipole moment and the minimum electrostatic energy[28]. The relevant results are summarized in table V-4.

Comparing the calculated principal axes and the experimental direction of the magnetic field at the Cl_{II} nucleus with the two possible values of θ we have to conclude that neither value is in marked disagreement with our results.

A comparison of the experimental and calculated orientations of the principal axes at the Cl_I and Cs sites (whose experimental determination will be considered in the next paragraph) shows that the results of a monopole calculation are in remarkable agreement with the experiments. The same can be concluded about a comparison between the experimental ratio of the two chlorine pure quadrupole frequencies (1.47) and the calculated one. (1.40).

5.5 The cesium resonance

a) Local magnetic fields at the Cs nuclei.

Figure V-11 shows a typical resonance diagram for the Cs^{133} nuclei. The data were taken at a temperature of 4.2°K in an external field of 5.320 kOe. Each resonance actually consists of seven components (figure V-12) which results from a small quadrupole effect. By considering the $|-\frac{1}{2}) \overset{\leftarrow}{\rightarrow} |+\frac{1}{2})$ transition one finds (neglecting quadrupole effects beyond the second order) that the internal fields lie in the a - b plane at 24° from the b axis. The results are summarized in the stereogram of figure V-13 and table V-3.

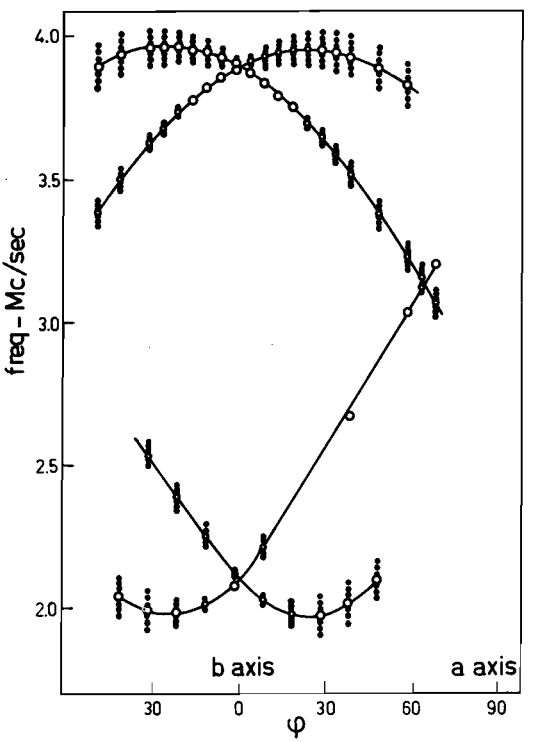

Fig.V-11 Angular dependence of the splitting of the Cs resonance in an external field of 5320 Oe. at 3.0 K. The curve is drawn through the $-\frac{1}{2} \rightarrow +\frac{1}{2}$ transition, the other transitions are represented by dots.

The magnitudes of the internal fields can be found by measuring the maximum splitting of the $|-\frac{1}{2}) \rightleftarrows |+\frac{1}{2})$ transition in the a-b plane, which should be twice the internal field, or by applying the relation

$$H_{int} = \{ \left(\frac{2\pi}{\gamma} \nu_{\perp} \right)^2 - H^2_{ext} \}^{\frac{1}{2}} \qquad (V\text{-}5)$$

in which $\nu_{\perp}$ stands for the frequency where the components cross. Monitoring this crossing on the scope as a function of temperature did result in the temperature dependence of the internal field at the Cs sites shown in figure V-14.

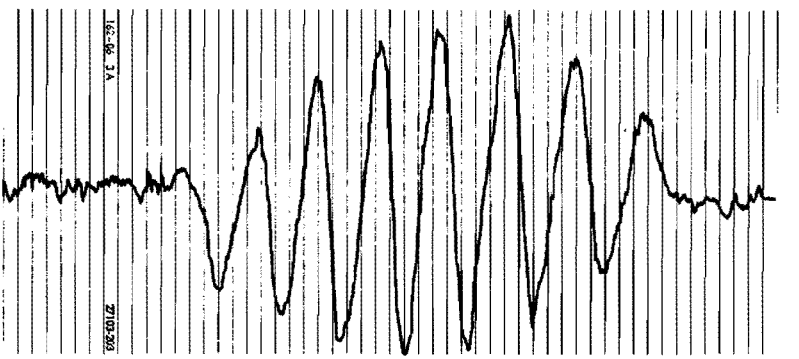

Fig.V-12 Recorder output, showing the first derivative of the quadrupole splitted Cs resonance line. The frequency intervals between the vertical lines are 3 kc/sec.

The large component of the internal field along the b-axis at a Cs site suggests that it contains a large contribution from an isotropic transfer hyperfine interaction. Dipole calculations will show that this is indeed the case (Table V-7).

b) Electric field gradient tensor at the Cs sites.

In chapter IV a method was described to determine the principal axes of the electric field gradient tensor in a high field case. Application of this technique to the Cs nuclei in Cs Mn $Cl_3.2H_2O$ resulted in the orientations tabulated in table V-4. The experiments were performed at hydrogen temperatures in an external field of about 5000 oersted. One of the principal axes coincides with the c axis, which could be expected because of the special positions of the Cs nuclei on a two fold axis. In the antiferromagnetic state the orientation of the principal axes of the E.F.G. tensor can be determined from the rotation diagram in figure V-11.

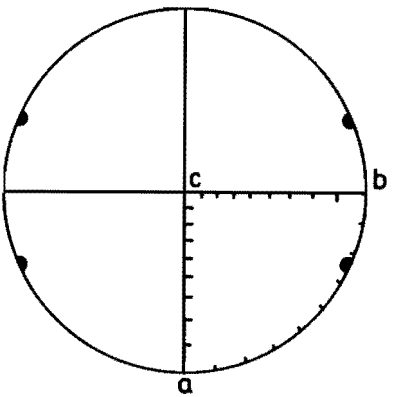

Fig.V-13 Stereogram showing the orientation of the local fields at the Cs nuclei.

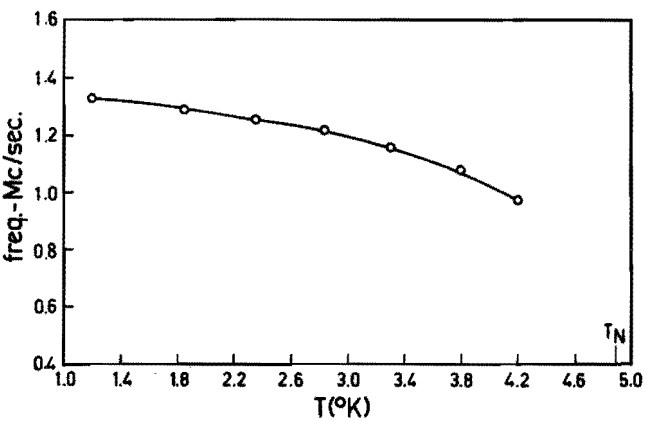

Fig.V-14 Temperature dependence of the Cs resonance frequency.

If we plot the angular dependence of the overall width of the quadrupole splitting (figure V-15), the extrema in this graph will correspond to the situation where the total field on the nuclear site coincides with one of the principal axes of the E.F.G. tensor. The direction of the total field can be found by adding the known internal field to the externally applied field. The results agree completely with those found in the paramagnetic state. A comparison of the magnitude of the splitting with the theoretical formulas given in section 5.4 leads to the same agreement for η .

5.6 The proton resonance.

Figure V-6 shows the temperature dependence of the internal fields found at the two types of proton sites. The directions of the internal fields are shown in stereographic projection in figure V-16 and are tabulated in table V-5. The magnetic space group of the crystal will

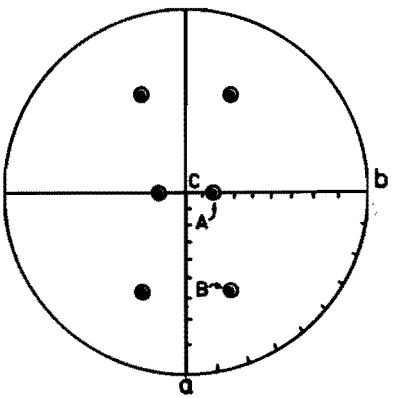

Fig.V-15 Angular dependence of the quadrupole splitting shown in Fig.V-11.

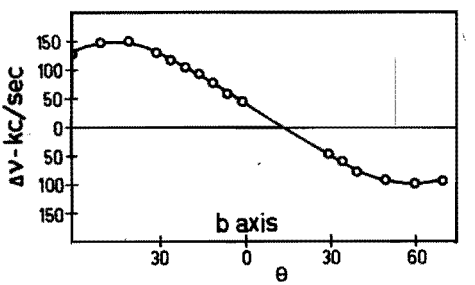

Fig.V-16 Stereogram showing the orientation of the local fields at the proton sites. The highest field is indicated with A, the lower field with B.

be considered in some detail in the next section. However, previous to doing this it is worthwhile to note that two important suggestions about the nature of the magnetic space group can be obtained simply by inspecting figure V-16.

Table V-5 Comparison of observed and calculated fields at proton sites

	Field orientation* - A sites			Field orientation* - B sites			B_A/B_B
	α	β	γ	α	β	γ	
observed	90.0	71.5	18.5	38.5	67.0	61.0	1.04
P_{2b} cca	76.3	85.2	14.5	24.5	78.9	68.5	0.66
P_{2b} c'ca'	83.5	73.5	17.8	31.5	72.3	64.8	1.02

* Angles from the a,b,c crystallographic axes.

For our first remark we will refer to the selection procedure of the magnetic space group outlined in section 2.2. Figure V-16 shows that the aspect group of the crystal is mmm, $N_a = 8$ and $N_f = 2$. From the room temperature crystallographic data we obtain $N_n = 16$. Therefore $N_a.N_f/N_n = 1$ applies to this case. Thus only in the situation that the magnetic space group contains no inversions the magnetic and chemical unit cell are identical. The magnetic point groups which meet this condition are mmm1', m'm'm' and m'mm.
One further hint as to the nature of the magnetic space group from figure V-16 stems from the observation that the vectors for the high field A sites lie in the b - c plane quite close to the c axis. Since the field at the proton nuclei is presumably dipolar in origin, this observation implies that such a proton site is located at least approximately in the plane of two antiparallel spins which are displaced along the c axis. From figure V-2 it is clear that the protons which bond the structure together along the c axis can approximately satisfy this condition. It therefore follows that antiferromagnetic ordering along the c axis is quite likely.

5.7 The magnetic space group.

As we already mentioned in section 5.2, both Cs-, Cl- and Mn-nuclei occupy special positions in the chemical unit cell. Because special positions restrict the possibilities for the orientations of fields, we may expect to get information about the magnetic space group by comparing the admissible directions of the local fields with the experimentally obtained data. In magnetic space groups the admissible directions of axial vector on twofold axes are (section 2.2):

a) on 2(an ordinary twofold axis)... parallel to the axis.

b) on 2'(an anti-twofold axis)..... perpendicular to the axis.

The second column of table V-6 shows the twofold axes which pass through the Cl_I, Cs and Mn sites in the chemical unit cell. By considering the direction of the axial vectors $\vec{B}$ and $\vec{M}$ (internal magnetic field and magnetization) at these sites, given in the third column, we arrive at the type of twofold axis which must exist at these positions in the magnetic space group. This result is tabulated in the last column of table V-6.

Table V-6 Axes of the magnetic space group

Site in chemical unit cell	Axis in chemical unit cell	Direction of $\vec{B}$ or $\vec{M}$	Axis in magnetic unit cell
Cl_I	2_z	z	2_z
Cs	2_z	$\perp$ to z	$2'_z$
Mn	2_y	y	2_y

The left part of figure V-17 shows the locations of some Cl_I, Cs and Mn sites projected on the a-b plane. At the right in the figure are shown the locations of the corresponding axes of the magnetic space group. Primed or anti-axes are shown in white while unprimed or ordinary axes are shown in black. The primed screw axes along a arise from the product of the twofold axes along b and c. The alternation of primed and unprimed twofold axes along b requires that the magnetic cell must contain an anti-translation along b. Thus the left hand portion of figure V-17 shows only one half of the magnetic unit cell. As noted in the last paragraph the proton resonance data alone implies the likelihood of such an anti-translation but it does not suggest its direction. There are only two magnetic space groups which have arrangements of axes and anti-translations corresponding to the present situation. In the notation of Opechowski and Guccione[33] these are designated as $P_{2b}cca$ and $P_{2b}c'ca'$. In the Belov[40] notation the first of these groups is designated by $P_b cca$ while the second appears only with the permutation (a,b,c) → (b,c,a) and is written as $P_c nna$. Diagrams of these two groups can be found in Koptsik's book[41] as Ш^{347}_{54} and Ш^{316}_{52}. The two groups differ in that the primed and unprimed c axis glide planes are interchanged. As a result the Mn spins at z = $\frac{1}{4}$ and z = $\frac{3}{4}$ must be parallel if the group is $P_{2b}cca$ or they must be anti-parallel if the group is $P_{2b}c'ca'$.

Since the two layers at z = $\frac{1}{4}$ and z = $\frac{3}{4}$ are linked by hydrogen bonds one may effect a choice between the two groups by comparing the observed direction and magnitude of the internal fields at the proton sites with the corresponding computed fields based on the two possible groups. The value of the average magnetic moment of the Mn ions is needed in

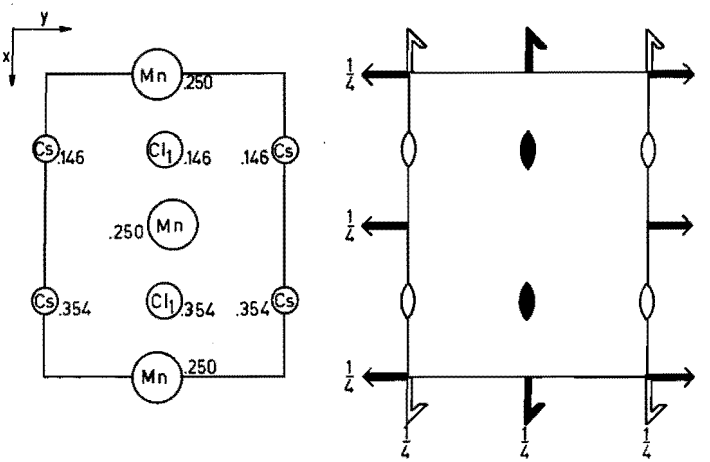

Fig. V-17 The left-hand diagram shows the postion of the nuclei used to determine the nature of the twofold axes. The right-hand diagram shows the axes determined by the experiments. Standard crystallographic symbols for the axes have been used with the added convention that a black axis is an ordinary axis and a white axis is an antiaxis. The figure at the right represents only one-half of the magnetic unit cell.

such a computation if one is to calculate anything but the relative magnetitudes of the internal fields. In work on other manganese chlorides it has been assumed that the temperature dependence of the average magnetic moment was of the same form as the temperature dependence of the proton internal fields, because both dipole magnetic interaction and hyperfine interaction are supposed to be proportional to the average Mn magnetic moment. The scale factor was determined by extrapolating the temperature dependence function to $0^{o}K$ and requiring that at this temperature the Mn moment be equal to five Bohr magnetons. In this case such an extrapolation is not valid since the susceptibility data of Smith and Friedberg indicates the onset of different magnetic behaviour below $0.35^{o}K$. Consequently in the present case we must content ourselves with a comparison of orientation and relative magnitudes. The actual dipole sums required in the computations extended over 5000 Mn ions surrounding a given proton site. The experimental and calculated results are given in table V-6. Although the agreement is not perfect the ratio B_A/B_B clearly shows that the correct magnetic space group is $P_{2b}c'ca'$. Figure V-18 shows the spin arrangement that follows from the magnetic space group $P_{2b}c'ca'$ and the magnetization along b.

In the previous paragraphs we made some comments about the order of magnitude of the hyperfine fields at the Cl_I, Cl_{II} and Cs sites. We had to postpone the calculation of the hyperfine field at these sites until we could calculate the dipolar contribution to the total internal field.

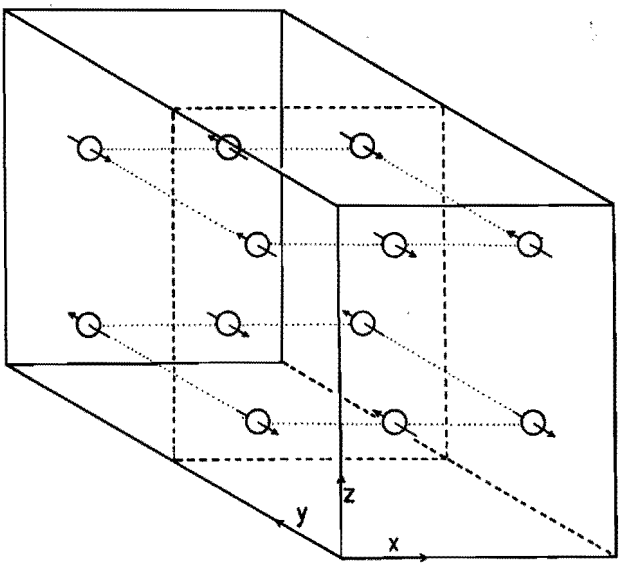

Fig.V-18 The spin arrangement in $CsMnCl_3.2H_2O$.

Having determined the space group it is now possible to determine the magnetic moment at any given temperature from the proton internal fields. The magnetic moment thus obtained may then be used to calculate the dipolar component of the internal fields at other sites. The transferred hyperfine field is then obtained by subtracting (vectorially) the dipolar field at these sites. Table V-7 gives the values of the dipolar and transferred fields at the Cl_I, Cl_{II} and Cs sites at T = 1.8°K. The calculated fields are based on a magnetic dipole moment of 3.55 Bohr magneton at T = 1.8°K and 3.73 Bohr magneton at 0°K. So in order to match the proton dipole fields we have to assume a spin reduction of about 25% at 0°K. For the sake of completeness the values of the parameters which characterize the quadrupole interaction are also given in table V-7

Table V-7 Internal fields and quadrupole interaction parameters for Cl_I, Cl_{II} and Cs nuclei.

nucleus	dipolar field	transferred h.f.field	% trans.hyp.field along b axis
Cl_I	0.46	0.2	0
Cl_{II}	3.48	21.20	99.6
Cs	1.37	2.23	98.2

Quadrupole interaction parameters.

nucleus	pure quadrupole res.freq*.(Cl^{35})	$\frac{e^2Qo}{h}$	asymmetry parameter η	orientation** internal field θ	ϕ
Cl_I	6.15	12.2	0.30	90	0
				43	-
Cl_{II}	4.85	-	-	or	
				55	-
Cs	-	0.35	0.33	23.5	0

* - Mc/sec

** with respect to the axes of the E.F.G tensor.

5.8 Exchange interactions.

The magnetic space group of $CsMnCl_3.2H_20$ reveals that all the nearest neighbour interactions are antiferromagnetic and consequently the exchange integrals are negative. From the susceptibility measurements reported by Smith and Friedberg[23] it has been shown that in order to explain the data with a linear chain model one has to assume an intra-chain exchange coupling constant J_1/k of -3.1^oK.
The molecular field approximation for the Néel temperature is

$$kT_N = \frac{-2\ S(S+1)}{3}\ 2\{J_1 + J_2 + J_3\}\ , \qquad (V\text{-}6)$$

where J_1 is the intra-chain exchange integral and J_2, J_3 the inter-

chain exchange integrals along y and z directions. A calculation of the Néel temperature from (V-6) with $J_1/k = -3.1^{\circ}K$ would yield $T_N \geq 36^{\circ}K$ which is far too large compared with the observed $T_N = 4.89^{\circ}K$. A calculation of the Néel temperature by Spence[22] based on Green's function theory gives a more reasonable result.

CHAPTER VI

NUCLEAR MAGNETIC RESONANCE IN $KMnCl_3 . 2H_2O$.

6.1 Crystallography

The existence of the salt $KMnCl_3.2H_2O$ was first published by Saunders[25] who reported the structure to be triclinic. A recent x ray study by Jensen[29] et.al. established the space group to be $P\bar{1}$ with two formula units per chemical unit cell. The atomic parameters are tabulated in table VI-1.

Table VI-1 Room-temperature lattice parameters and atomic coordinates of $KMnCl_3 2H_2O$.

$P\bar{1}$	a = 6.49 Å α = 96.8	b = 6.91 Å β = 114.1	c = 9.91 Å γ = 112.6
position	a	b	c
O_I	0.7739	0.7853	0.5111
O_{II}	0.6989	0.4026	0.1663
Cl_I	0.2504	0.7112	0.4984
Cl_{II}	0.6501	0.8929	0.1877
Cl_{III}	0.1725	0.3353	0.1686
Mn	0.9517	0.2972	0.3254
K	0.1394	0.8468	0.1963
H_I	0.6192	0.7588	0.5192
H_{II}	0.7561	0.8205	0.4141
H_{III}	0.6206	0.3145	0.0560
H_{IV}	0.5627	0.4003	0.1882

The structure is made up of units consisting of two octahedra with a bridge of two shared chlorines in between. The two octahedra in one unit are related by an inversion center situated between the manganese ions as is shown in figure VI-1. We will refer to the equivalent

chlorine positions shared by the two octahedra as Cl_I positions. The two inequivalent chlorines at the ends will be denoted as Cl_{II} and Cl_{III}. The hydrogen positions are not known exactly. Following the suggestion of Jensen[29] they should be placed on the two shortest O -- Cl bonds.

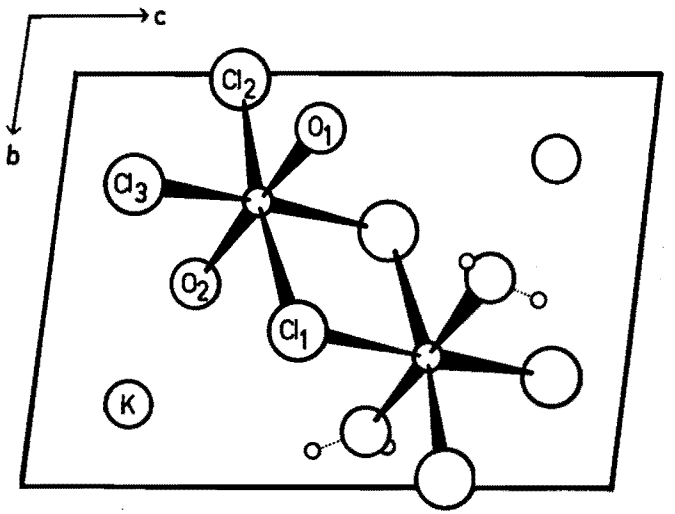

Figure VI-1 The structure of $KMnCl_3.2H_2O$. Only one set of hydrogens is shown.

However, in $KMnCl_3.2H_2O$ the angle Cl -- O -- Cl is much smaller then 108° which is the preferred angle of an H-O-H molecule. Therefore one might conjecture that the hydrogens are displaced somewhat in the Cl -- O -- Cl plane, such that the angle H-O-H becomes 108° and the bonding distance is 0.987, as suggested by El Saffar[27]. The resultant hydrogen coordinates are given in table VI-1. In spite of nummerous attemps the positions couldn't be checked experimentally by measuring the magnitude and direction of the proton-proton vector through dipole-dipole interaction nor by determining the principal axes of the electric field gradient tensor at the deuteron nucleus in $KMnCl_3.2D_2O$, as we did for $CsMnCl_3.2D_2O$. A computer calculation based on the minimum of electrostatic energy (see section 2.3) showed a satisfactorily agreement with the conjectured positions as may be seen from the comparison of table VI-2 with table VI-1.

Table VI-2 Calculated proton positions with electrostatic minimum energy

position	a	b	c
H_I	0.6148	0.7519	0.5118
H_{II}	0.7619	0.8189	0.4167
H_{III}	0.6194	0.3276	0.0553
H_{IV}	0.5857	0.4463	0.1857

The morphology of the crystals varies, but the (001) is mostly well developed. As an example figure VI-2 shows a crystal shape which is often seen.

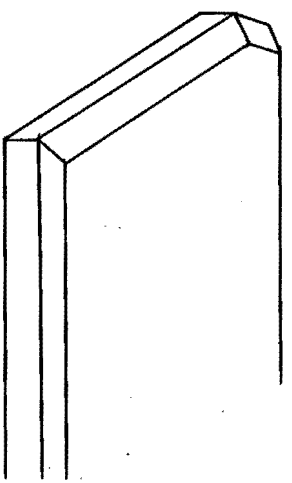

Fig. VI-2 The crystal shape of $KMnCl_3.2H_2O$ most commonly obtained.

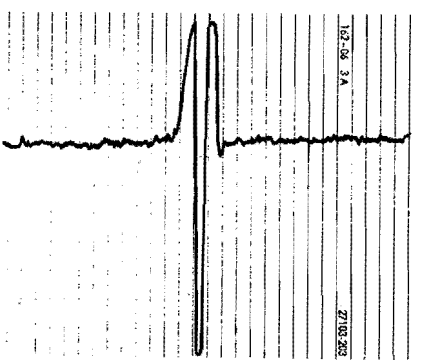

Fig. VI-3 Second derivative of a Cl^{35} signal observed in $KMnCl_3.2H_2O$ at 1.1 K. The width of the line is about 15 kc/sec.

6.2 Preparation and detection

Single crystals of $KMnCl_3.2H_2O$ were grown by evaporation at room temperature from a saturated solution of KCl and $MnCl_2 4H_2O$, in molecular ratio 1 : 2, solved in water. Out of a solution with equal molecular weight of the constituents, the KCl crystallized first till

the molecular ratio in the solution was about as stated above, after which crystals of $KMnCl_3.2H_2O$ began to grow. However, when the percentage of KCl was lowered enough by this crystallization process, $MnCl_2.4H_2O$ crystals began to appear. Therefore we checked the composition of the crystals before the experiments. The large crystals had typical dimension of about 3 x 8 x 20 mm. and did not show very well developed faces on the ends.
The signals in the antiferromagnetic state, especially those from the chlorines were very good. Signal to noise ratio's of about 1 : 50 could be obtained at low temperatures without much trouble. A typical recording is showed in figure VI-3. In the paramagnetic state, however , the signals of the chlorines were very poor.

6.3 Chlorine resonance.

a. Temperature dependence.
Figure VI-4 shows the temperature dependence of the observed Cl^{35} transition frequencies. The Cl^{37} transitions form a similar set somewhat lower in frequency. As expected on the basis of the reported structure, there are nine zero field lines which have to be divided in three sets, belonging to the three inequivalent Cl positions in the chemical cell. As we already saw in the case of $CsMnCl_3.2H_2O$ (chapter V-2), one of two possibilities applies for the shared Cl_I positions; either the, presumably isotropic, transferred hyperfine field is very small or it is about twice the value we expect for a single bonded chlorine, such as Cl_{II} and Cl_{III}, depending on whether the two coupled Mn spins are parallel or antiparallel. Unlike the $CsMnCl_3.2H_2O$, where the field at the Cl_I nucleus is very small, we may divide the transition frequencies in $KMnCl_3.2H_2O$ in one set of six lines which are centered around 9 Mc/sec. and a set of three lines which are clearly centered around a frequency about twice this value. Thus our first conjecture is that the Mn spins in one unit are parallel. We will discuss this fact later on.
As one can see from the data plotted in figure VI-4, only two resolved Cl^{35} pure quadrupole resonances were observed in the paramagnetic state. In spite of several attemps we did not succeed in finding the third one. This will have serious drawbacks in the selection of the frequency sets as we shall see later on. The two pure Cl^{35} quadrupole resonances were found at 5.21 Mc/sec. and 4.24 Mc/sec.. As the paramagnetic proton signals disappeared at $T = 2.75^{o}K$, we quote as our result that the anti-

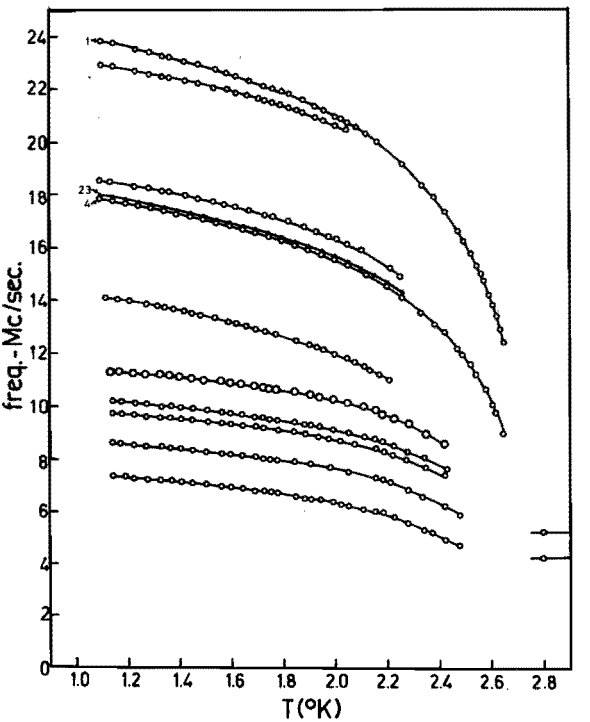

Fig.VI-4 Temperature dependence of the Cl^{35} and the proton lines. The four proton resonances are marked with numbers 1-4. The lines 2,3 and 4 lie very close together, only the data points of line 4 are drawn. The fifth line from the bottom consists of two resonances whose frequency difference is approximately 60 kc/sec.

ferromagnetic transition temperature will be close to this value.

b) Magnetic fields at the chlorine nuclei.

The magnitude and direction of the local magnetic fields at the Cl^{35} nuclei can only be found from the expressions (II-3) and (II-7) when the labeling of the frequencies is known. This problem is complicated in this case by the fact that we have to select first the sets of three transitions originating from one equivalent Cl position before we can start with labeling the frequencies. Because our first interest is the determination of the magnetic space group, we are particularly

interested in the direction of the sublattice magnetization, which we need for our dipole field calculations. Since we assume the transferred hyperfine interaction to be largely isotropic, the direction of the local magnetic field at one nucleus will probably give a reasonable indication of the orientation of the sublattice magnetization. We may try then to observe a spin flopping which will reveal the real direction of $\langle\vec{\mu}\rangle$.

We will now concentrate our attention to the three lines at high frequencies because there is a strong indication, as we mentioned in the preceding subsection, that these lines originate from one chlorine position i.e. the Cl_I nucleus. In the following we will sample the experimental data and try to find the experimental evidence to support this view.

In chapter II we summarized some selection procedures. Among these the extrapolation of Γ_2 and Γ_3 plots versus ν^2_{proton} played an important part because they are exact and generally valid. However, they cannot be used here because the inequivalent protons in the unit cell show a different temperature dependence. We will return to this subject in section 6.4.

An interesting feature of the high frequency lines is that the frequency differences between the outer lines and the middle one are the same within the experimental error and independent of temperature (or magnetic field). Inspection of the second order perturbation expressions for ν_i learns that consequently the second order terms which contain the field dependence of the frequency differences must be very small. This is the case for θ near zero degrees. At the same time this fact is in favour of the proposition that these lines belong to one set where it is not very likely that lines originating from different nuclei with different local magnetic fields exhibit such a constant frequency difference.

If we are dealing with the case $\theta = 0$ the middle line must be ν_2 and the frequency difference with the other lines will equal ν_{Qo}. This frequency difference is 4.34 Mc/sec.. Indeed we measured a pure quadrupole transition in the paramagnetic state near this value at 4.24 Mc/sec.. However, we must realize that this equals $\nu_{Qo}(1 + \frac{\eta^2}{3})^{\frac{1}{2}}$. The difference between the value of ν_{Qo} in the paramagnetic and the antiferromagnetic state (which may be as high as 600 kc/sec. if η is large) must be due to a slight change of the spatial charge distribution which is not unusual.

Table VI-3. Results of point charge calculation of the electric field gradient for the chlorine sites in $KMnCl_3.2H_2O$ (in units of e . 10^{24} . . $(1 - \gamma_\infty)cm^{-3}$) and a comparison with the experimental ν_Q. The theoretical ν_Q is calculated on the basis of $\gamma_\infty = -18.8$. The orientation is given with respect to a rectangular coordinate system xyz ; x=a, y in a-b plane.

nucleus	principal axis	principal value	orientations α	β	γ	calc.ν_Q (Mc/sec.)	Exp.ν_Q (Mc/sec.)
Cl_I	x	+0.0462	80	38	144		
	y	+0.1072	142	76	56	4.28	
	z	-0.1534	54	125	54		
Cl_{II}	x	-0.0665	104	50	136		4.24
	y	-0.0874	18	89	108	4.19	
	z	+0.1539	101	140	128		
Cl_{III}	x	-0.0751	126	63	132		
	y	-0.1151	85	31	60	5.21	5.21
	z	+0.1902	36	77	123		

A monopole calculation of the electric field gradient tensor (section 5.4) resulted in the values tabulated in table VI-3. As was shown by several authors[11,36] the results of such a calculation may be trusted as far as the orientation of the principal axes and the ratio of the magnitudes of V_{zz} belonging to inequivalent positions are concerned. From table VI-3 one sees that a combination of the theoretical ratios of the three ν_Q with the two observed resonances leads to the conclusion that the resonance at 4.24 Mc/sec. realy consists of two lines which coincides accidentally. The direction of the principal z axis of the Cl_I is plotted in figure VI-5 together with the gradients of the three frequencies and the local field direction $\vec{B}$, determined with (II-7) and the assumption that the middle line is ν_2. The angle θ between $\vec{B}$ and the z axis is 8 degrees which agrees with the pure experimental evidence. From the fact that the directions of the gradients do not exactly coincide and that the reduced magnitudes are not very close to unity (table VI-4) one can conclude that the experimental data also provides evidence that θ can not be exactly zero.

Another consequence of the situation where θ is small is that $\nu_2 \cong \nu_Z$. The ratio $\nu_2(Cl^{35})/\nu_2(Cl^{37})$ should be very near 1.202 (section 2.4) and

$\nu_1(Cl^{35})/\nu_1(Cl^{37})$ and $\nu_3(Cl^{35}/\nu_3(Cl^{37})$ can be calculated with (II-12). A comparison between these three values and the experimental data in table VI-4 shows a remarkable good agreement.

Table VI-4. Summary of the gradients of the chlorine lines in $KMnCl_3.2H_2O$ and the ratio of the frequencies of the two chlorine isotopes. In the last two columns a division of the transition frequencies in sets arising from one nuclear site and their labeling within a set is suggested.

ν_i*	$\frac{\nu_{i(Cl^{35})}}{\nu_i(Cl^{37})}$	$2\pi/\gamma\lvert\nabla_B\nu_i\rvert$	orientation $\vec{\nabla}_B\nu_i$** α	β	γ	nucleus	label
22.800	1.214	1.16	60	132	56		ν_3
18.450	1.201	1.16	62	135	58	Cl_I	ν_2
14.100	1.183	1.17	68	140	59		ν_1
11.360	1.211	1.08	57	132	60		ν_1
10.275	1.205	1.05	63	138	61	Cl_{II}	ν_2
8.679	1.197	1.21	77	160	76		ν_3
11.305	1.208	1.10	49	131	69		ν_1
9.821	1.208	1.02	55	130	60	Cl_{III}	ν_2
7.421	1.188	1.27	103	128	41		ν_3

* in Mc/sec. at 1.15°K

** with respect to a rectangular coordinate system xyz
x = a, y in a-b plane.

Considering the arguments given above, we conclude that the suggested labeling is correct and that the two coupled Mn spins are parallel.
A search for the zero frequency spin flopping near the direction of the local magnetic field at the Cl_I nucleus was sucessfull. The spin flopping was observed at 1.1°K with a magnetic field of 11.7 kOe. in the direction as shown in figure VI-5 and tabulated in table VI-5.
Once the sublattice magnetization direction and the relative orientation of the two coupled Mn spins are known, we have enough experimental data extracted from the chlorine resonance to be able to proceed with the magnetic space group determination. It is for this reason that we didn't

bother too much about the labeling of the low frequency chlorine sets. Nevertheless a suggestion of a possible labeling based on the gradients, (fig.VI-5b) the Cl^{35}/Cl^{37} ratios and the selection criteria mentioned in section 2.4 is shown in table VI-4.

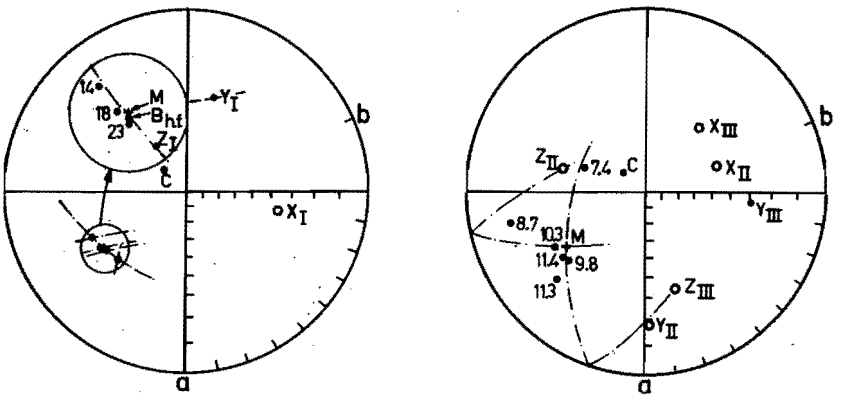

Fig.VI-5 Stereograms showing the gradients $\vec{\nabla}_B \nu_i$ (denoted by their approximate frequencies), the principal axes of the E.F.G. tensor at the chlorine sites (X_i, Y_i, Z_i) and the sublattice magnetization M. In the stereogram on the left side the direction of the hyperfine field at the Cl_I nucleus is also plotted.
The planes passing through M and Z_i are the planes in which the gradients of the Cl_i transitions would lie if η were zero and the local fields at the nuclei were exactly along M. (i=I, II or III).

Table VI-5 Showing the relative orientations of sublattice magnetization and the hyperfine field at the Cl_I nucleus with respect to a rectangular coordinate system xyz; x = a, y in a-b plane.

	orientation		
	α	β	γ
sublattice magnetization	62	133	56
hyperfine field at Cl_I	61	133	56

6.4 The proton resonance

The temperature dependence of the four proton lines is shown in figure VI-4, the orientation is plotted in stereogram VI-6 and tabulated in table VI-6. In the preceding section we mentioned already the unusual behaviour of the proton lines. In figure VI-7 this effect is illustrated by a graph showing the ratio of the highest and the lowest proton frequency versus temperature, which should be constant in the assumption that both proton sites experience a local field proportional to the sublattice magnetization. The most plausible explanations of this effect are:

a) a gradual change of orientation of the magnetic moment on the Mn ions in the antiferromagnetic state with temperature.

b) a slight displacement of the proton positions in the unit cell in the antiferromagnetic state with temperature.

Two experiments were performed to check these possible explanations. The first one seems to be unlikely because, within the experimental error ($\pm$ 1°) no change in the local field orientation on the protons can be observed with temperature. The second explanation doesn't seem to be correct because a change in position would undoubtely reveal itself in the quadrupole interaction measured on the deuterium nuclei in $KMnCl_3.2D_2O$.

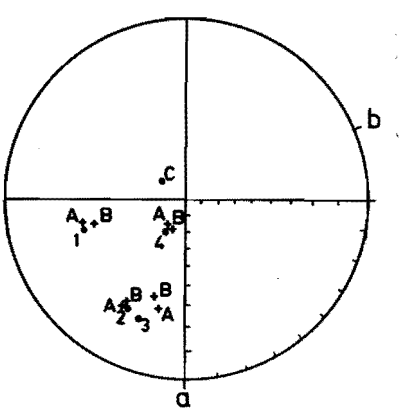

Fig.VI-6 Stereogram showing the observed and calculated local fields at the hydrogen nuclei.
o - corresponds to the observed fields.
+ - corresponds to the calculated fields.
The numbers refer to the lines indicated in fig.VI-4. $A = P_a \bar{1}$; $B = P_{a+c} \bar{1}$.

The temperature dependence of the quadrupole splitted deuterium lines is shown in figure VI-8. The quadrupole splitting stays constant in the temperature range within the experimental error of 2 kc/sec.

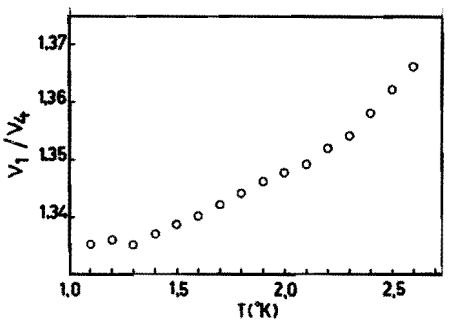

Fig.VI-7 Temperature dependence of the ratio of the highest and the lowest proton frequency.

6.5 The magnetic space group.

From the experimental data it follows that the symmetry of the aspect group is $\bar{1}$ and the number of distinct field magnitudes is 4. The room temperature crystallographic structure leads to 8 protons per lattice point. Therefore $N_a \cdot N_f / N_n = 1$ and, according to section 2.2, the magnetic space group contains an anti-translation unless no inversion is present. However, from the chlorine resonance it is clear that the inversion center relating the two Mn spins in the two coupled units is uncolored and so the magnetic space group must contain an anti-translation.

The only space group which meets this condition is $P_s \bar{1}$. The subscript denotes the existence of an elementary anti-translation. The colored translation is not necessarily one of the translations we used to describe the crystallographic structure. However, it can always be generated by a combination of anti-translations along the edges of our arbitrary unit cell. To decide what combination has to be taken one has to perform a dipole calculation of the magnetic field at the proton sites based on each of the seven possible combinations and compare these results with the experimentally obtained data.

In the calculations the magnetic moment of the Mn ions was assumed to be 5 Bohr magnetons at $0^{\circ}K$. Their direction was taken as the direction

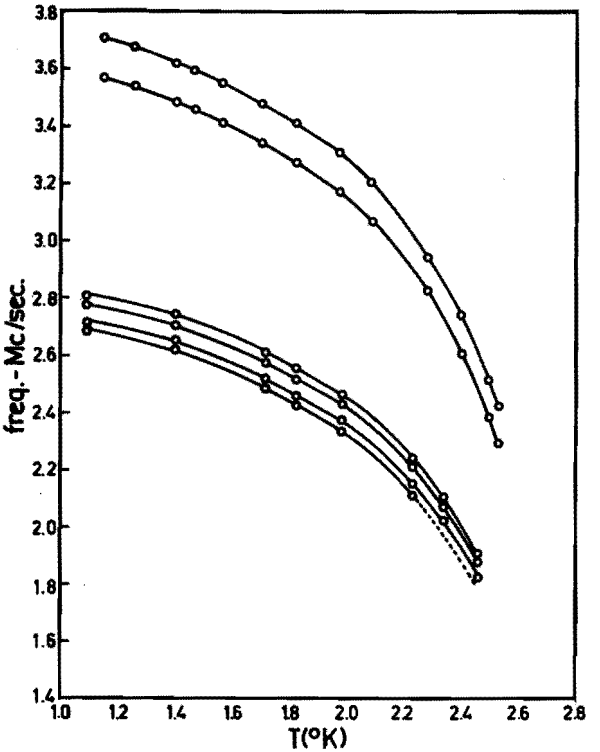

Fig. VI-8 Temperature dependence of the deuterium lines in $KMnCl_3.2D_2O$.

of the sublattice magnetization as deduced from the spin flopping experiment described earlier. The proton positions were taken as tabulated in table VI-1. The dipole sum was extended over more than 3000 Mn ions surrounding a given proton site. The results of the two calculations which fit far out best the experimental data are shown in figure VI-6 and are tabulated in table VI-6. Neither slight changes in the magnetization direction nor changes in the, still somewhat uncertain, proton positions seemed to improve the agreement of one of the two possible spin arrangements with the experimental data.
Therefore we conclude that the magnetic ordening in $KMnCl_3.2H_2O$ can be described by the space group $P_a\,\bar{1}$ or $P_{a+c}\,\bar{1}$. The exchange coupling between the two chlorine coupled Mn ions is ferromagnetic and the sublattice magnetization direction is inclined 20 degrees from the Mn - O bond direction.

Table VI-6. Comparison of experimental proton fields with those calculated on the basis of an a and an a+c anti-translation. Orientations with respect to a rectangular coordinate system xyz; x=a, y in a-b plane.

proton	Orientation									ratio		
	observed			calculated with $P_a\bar{1}$			calculated with $P_{a+c}\bar{1}$			obs.	$P_a\bar{1}$	$P_{a+c}\bar{1}$
	α	β	γ	α	β	γ	α	β	γ			
1	76	146	60	78	148	61	78	144	56	1		
2	35	115	67	37	116	66	37	115	64	1.29	1.21	1.24
3	29	110	70	30	103	64	36	106	58	1.30	1.21	1.18
4	70	103	25	75	101	19	72	99	21	1.34	1.20	1.16

6.6 Miscellaneous remarks.

As we saw in the preceding section, no decisive choice could be made, through dipole calculations, between the space group $P_a\bar{1}$ and $P_{a+c}\bar{1}$. The results of both dipole calculations differ about the same from the observed magnitudes and directions of the local fields at the hydrogen nuclei(Table VI-6). Small deviations like these are quite common when one compares the calculated dipole fields with the observed ones. The reason for this must be sought in the spatial distribution of the magnetic moment. Van Ormondt[30] showed that in $[Mn(H_2O)_6]^{++}$ complexes the unpaired spin density at the hydrogens is such that it can account for a hyperfine field at the hydrogens of a few hundred Oersted. The unpaired spin density at the oxygen is probably responsible for those deviations which can not be explained by the first argument.
One may argue that it must be possible to correct the dipole sums for these effects, using the values measured by van Ormondt. However, this would not bring about a decision between the space groups because the corrections for both are the same. In general it may be worthwhile in those cases where the proton positions and the sublattice magnetization direction are well known, to estimate the contribution from the hyperfine effects by taking the difference between the observed and the calculated fields.

In his review article on the theory of exchange in insulators, Anderson[42] indicates that in the case of a so-called 90° exchange through a ligand, one might expect an increasing importance of the antiferromagnetic exchange terms going from the configuration d^8 to d^5.
In $KMnCl_3.2H_2O$ the Mn-Cl_I-Mn' angle is about 90°. The interaction, however, is ferromagnetic while in $CoCl_2.2H_2O$, where the coupling between the Co ions resembles the $KMnCl_3 2H_2O$ case, the interaction is antiferromagnetic. Apparently the relative large number of ferromagnetic terms in the exchange energy for Mn-compounds causes the sign of the interaction to be rather uncertain. A more complete comparison between the Mn salts investigated with nuclear magnetic resonance including $KMnCl_3.2H_2O$ and $CsMnCl_3.2H_2O$ can be found in reference [43].

SUMMARY

This thesis describes the results of nuclear magnetic- and quadrupole resonance experiments on some antiferromagnetic complex hydrated Mn(II) chlorides i.c. $Cs_2MnCl_4.2H_2O$, $CsMnCl_3.2H_2O$ and $KMnCl_3.2H_2O$.
In the first chapter the theoretical solutions of the Hamiltonian for mixed electric quadrupole and magnetic dipole interactions are reviewed as far as they are needed in the interpretation of the cesium and chlorine frequency spectra. Expressions are derived for the moments of the energy levels in terms of the observable frequencies and the interaction parameters.
In chapter II a general outline is given how to obtain the information about the magnetic space group, the local magnetic fields at the chlorine nuclei and the proton positions from the experimental data.
Chapter III describes some details about the experimental set up.
Chapter IV deals with the description of an experimentally convenient method for the determination of electric field gradient tensors at nuclei in the paramagnetic state. The theory is applied to the Cs nuclei in $Cs_2MnCl_4.2H_2O$.
Chapter V describes the experimental investigation of $CsMnCl_3.2H_2O$ with nuclear magnetic resonance. The Cl, Cs and H resonance is used to determine the magnetic space group.
As the Cs, Mn and one of the Cl nuclei occupy special positions, the possible magnetic field directions on these nuclei are correlated to the nature of the magnetic symmetry operators. Determination of the local fields in the antiferromagnetic state leads to a set of symmetry operators which restrict the choice of the magnetic space group to a set of two. With a dipole calculation of the magnetic fields at the hydrogen nuclei, the selection is completed. The magnetic space group is $P_{2b}c'ca'$ and all the nearest neighbour interactions are antiferromagnetic.
The sublattice magnetization direction is along the b axis and the Néel temperature as concluded from the disappearance of the local fields at the Cl nuclei is 4.89 K. From experiments in both the paramagnetic and the antiferromagnetic state, some of the quadrupole interaction parameters are determined. A comparison with monopole calculations gives a

reasonable agreement.

In chapter VI the magnetic space group of $KMnCl_3.2H_2O$ is determined. The structure is made up of units of chlorine coupled octahedra. The hyperfine field at the nucleus of the shared chlorine will be small when the two adjacent Mn moments are anti-parallel, as was observed in $CsMnCl_3.2H_2O$. The hyperfine field will be roughly twice the value observed when only one Mn interaction is operative, if the two coupled Mn spins are parallel. In $KMnCl_3.2H_2O$ the observed Cl^{35} frequency spectrum can be divided in three sets originating from the three non equivalent chlorine sites. One set clearly centers around a frequency about twice as high as the others. From this fact we conclude a ferromagnetic interaction between the coupled Mn spins. The triclinic magnetic space group which meets this condition is $P_s\bar{1}$. The remaining choice of generating anti-translations could be limited to $P_a\bar{1}$ and $P_{a+c}\bar{1}$; the other possibilities could be ruled out with a dipole calculation of the magnetic field at the hydrogen nuclei.

The sublattice magnetization direction was found from a spin flop experiment. The Néel temperature determined from the disappearance of the paramagnetic lines was 2.75 K.

SAMENVATTING

In dit proefschrift worden de resultaten beschreven van kernspin-resonantie-en quadrupoolresonantie-experimenten aan enkele antiferromagnetische gehydrateerde complexe Mn^{++} chlorides i.c. $Cs_2MnCl_4.2H_2O$, $CsMnCl_3.2H_2O$ en $KMnCl_3.2H_2O$.

In het eerste hoofdstuk wordt een overzicht gegeven van de oplossingen van de Hamiltoniaan voor gemengd electrische quadrupool- en magnetische dipool-wisselwerkingen, voor zover ze gebruikt kunnen worden bij de interpretatie van de cesium- en chloorspectra. De momenten van de energieniveau's worden uitgedrukt in de frequenties van de waargenomen overgangen en de interactieparameters.

In hoofdstuk II wordt geschetst hoe uit de experimentele gegevens informatie verkregen kan worden betreffende de magnetische ruimtegroep, de lokale magnetische velden ter plaatse van de chloorkernen en de protonposities.

Hoofdstuk III beschrijft enige details van de meetopstelling.

In hoofdstuk IV wordt een in experimenteel opzicht eenvoudige methode besproken, waarmee de elektrische veldgradiënten op een kern in de paramagnetische toestand bepaald kunnen worden. De methode wordt toegepast op de Cs kernen in $Cs_2MnCl_4.2H_2O$.

In hoofdstuk V worden de kernspin-resonantiemetingen aan $CsMnCl_3.2H_2O$ beschreven. De Cl, Cs en H resonanties worden gebruikt om de magnetische ruimtegroep te bepalen.

Daar de Cs, Mn en een van de Cl kernen speciale posities bezetten, zijn de magnetische velden op deze kernen qua richting gekoppeld aan het karakter van de magnetische symmetrie-operator ter plaatse. De bepaling van de lokale velden in de antiferromagnetische toestand leidt aldus tot een groep symmetrie-operatoren die de keuze van de magnetische ruimtegroep tot een tweetal beperkt. Met behulp van een dipoolberekening van de magnetische velden op de waterstofkernen kan de selectie worden voltooid. De magnetische ruimtegroep is $P_{2_b}c'ca'$ en de interacties tussen naaste buren is antiferromagnetisch.

De subroostermagnetisatie is gericht langs de b as en de Néel-temperatuur, volgend uit het verdwijnen van de lokale velden op de Cl kernen, is 4.89 K. Uit experimenten in de paramagnetische en de antiferromagne-

tische toestand konden enige quadrupool-interactieparameters worden bepaald. Een vergelijking met de resultaten van een monopoolberekening geeft een redelijke overeenstemming.

In hoofdstuk VI wordt de magnetische ruimtegroep van $KMnCl_3.2H_2O$ bepaald. De struktuur is opgebouwd uit eenheden welke bestaan uit twee door chloor-ionen gekoppelde oktaeders. Het hyperfijn-veld op de kern van het gemeenschappelijke chloor-ion zal klein zijn als de magnetische momenten van de gekoppelde Mn-ionen anti-parallel staan; zoals was waargenomen in $CsMnCl_3.2H_2O$. Wanneer de magnetische momenten parallel staan zal de hyperfijn-interactie ongeveer het dubbele bedragen van de interactie op een aan een oktaeder gebonden chloorkern. In $KMnCl_3.2H_2O$ kan het waargenomen frequentiespectrum van de Cl kernen worden verdeeld in drie groepjes afkomstig van de drie niet-equivalente posities. Het zwaartepunt van een van de drie groepjes ligt duidelijk twee maal zo hoog als van de beide andere. Hieruit mogen we concluderen dat er een ferromagnetische interactie bestaat tussen de Mn-ionen in de gekoppelde oktaeders. De trikliene magnetische ruimtegroep die aan deze voorwaarde voldoet, is $P_s\bar{1}$. De resterende keuze tussen de zeven genererende anti-translaties kan worden beperkt tot $P_a\bar{1}$ en $P_{a+c}\bar{1}$; de andere mogelijkheden worden uitgesloten op grond van dipool-berekeningen van de magnetische velden op de waterstofkernen.

De richting van de subrooster-magnetisatie wordt gevonden door middel van een kritisch-veld experiment. De Néel-temperatuur, bepaald uit het verdwijnen van de paramagnetische lijnen, is 2.75 K.

REFERENCES

1 . H.H. Cohen and F. Reif, Solid State Phys. 5, 321 (1957).

2 . R.G.Shulman and V Jaccarino, Phys.Rev. 108, 1219 (1957) .

3 . G.M. Volkoff, Canad. J. Phys. 31, 820 (1953).

4 . R.V.Pound, Phys.Rev. 79, 685 (1946).

5 . Y. Ting, R. Manring and D.Williams, Phys.Rev. 96, 408 (1954).

6 . C. Dean, Phys. Rev. 96, 1053 (1954).

7 . C.H.W.Swüste, Internal report T.H.E.

8 . R.M. Steffen, E.Matthias and W.Schneider, T.I.D. 15749 U.S.Dept. of Commerce (1962).

9 . L.C.Brown and P.M.Parker, Phys.Rev. 100, 1764 (1955).

10. P.M.Parker and R.D.Spence, Phys.Rev.160, 383 (1967).

11. W.J. O'Sullivan, W.W.Simmons and W.A.Robinson. Phys.Rev.140, A1759 (1965).

12. A. Narath, Phys.Rev. 140, A552 (1965).

13. R.D.Spence, J.A.Casey and V.Nagarajan. Phys.Rev. 181, 488 (1969).

14. N.C. Tombs and H.P.Rooksby, Nature 167, 364 (1951).

15. S.Greenwald and J.S.Smart, Nature 166, 523 (1950).

16. P.A. van Dalen, Thesis Eindhoven (1966).

17. R.D.Spence and P.A. van Dalen, Acta Cryst. A24, 494 (1968).

18. J.A.Cowen and W.H.Tantilla, Am.J.Phys. 26, 381 (1958).

19. W.J.M. de Jonge, G.N.Srivastava and P.M.Parker, J.Chem.Phys. 49, 2843 (1968).

20. R.D.Spence and V.Nagarajan, Phys.Rev. 149, 191 (1966).

21. S.J.Jensen, Acta Chem.Scand. 18, 2085 (1964).

22. R.D.Spence, W.J.M. de Jonge and K.V.S.Rama Rao, J.Chem.Phys. 51, 4694 (1969).

23. T.Smith and S.A.Friedberg, Phys.Rev. 176, 660 (1968).

24. H.Forstat, J.N. McElearny and N.D.Love (unpublished)

25. C.E.Saunders, Am.Chem.J. 14, 127 (1892).

26. S.T.Jensen, P.Andersen and S.R.Rasmussen, Acta Chem.Scand. 16, 1890 (1962).

27. Z.M. El Saffar, J.Chem.Phys. 45, 4643 (1968).

28. W.H.Baur, Acta Cryst. 19, 909 (1965) .

29. S.J.Jensen, Acta Chem.Scand. 22, 641 (1968).
30. D. van Ormondt, R. de Beer, N. Brouha and S. de Groot (to be published).
31. J.A.Cowen and C.Fairall (private communication).
32. A.C.Botterman, W.J.M. de Jonge and P. de Leeuw, Phys.Letters 30A, 150 (1969).
33. W.Opechowski and R.Guccione, Magnetism, G.T.Rado and H.Shul, Eds. (Academic Press Inc., New York, 1965), Vol.2A, Chap.3.
34. E.P.Riedel and R.D.Spence, Physica 26, 1174 (1960).
35. G.E.Pake, J.Chem.Phys. 16, 327 (1948).
36. B.Morosin and A.Narath, J.Chem.Phys. 40, 1958 (1964).
37. J.P.A.M. Hijmans (Private communication).
38. G.Soda and T.Chiba, J.Phys.Soc.of Japan 26, 249 (1969).
39. G.Soda and T.Chiba, J.Chem.Phys. 50, 439 (1969).
40. N.V.Belov, N.N.Neronova and T.S.Smirnova, Tr.Inst.Kristallogr ., Akad.Nauk SSSR 11,33 (1955).
41. V.A.Koptsik, Shubnikov Groups. Moscow Univ.Press. (1966).
42. P.W.Anderson, Solid State Physics (Edited by F.Seitz and D.Turnbull) Vol.14, Chapt. 2.
43. R.D.Spence and K.V.S.Rama Rao, J.Chem.Phys. (to be published.).

LIST OF SYMBOLS AND ABBREVIATIONS

N.M.R.	nuclear magnetic resonance
P.Q.R.	pure quadrupole resonance
N.Q.R.	nuclear quadrupole resonance
E.F.G.	electric field gradient
H	Hamiltonian.
B	magnetic induction
ν_Z	$\frac{\gamma}{2\pi} B$ (Zeeman frequency without any quadrupole interaction)
ν_{Qo}	$\frac{e^2qQ}{2I(2I-1)h}$
ν_Q	$\frac{e^2qQ}{2I(2I-1)h}\left(1 + \frac{\eta^2}{3}\right)^{\frac{1}{2}}$ (pure quadrupole transition)
η	$(V_{xx} - V_{yy})/V_{zz}$ (asymmetry parameter)
$\vec{\nabla}_B$	$\vec{i}\frac{\partial}{\partial B_x} + \vec{j}\frac{\partial}{\partial B_y} + \vec{k}\frac{\partial}{\partial B_z}$ (gradient)
ν_2	$\left\|+\frac{1}{2}\right) \overleftrightarrow{+} \left\|-\frac{1}{2}\right)$ transition in the high field labeling.
θ	the polar angle of $\vec{B}$ in the principal axes system of the E.F.G.
ϕ	the aximuthal angle of $\vec{B}$ in the principal axes system of the E.F.G.

STELLINGEN

I

De magnetische ruimtegroep van koperformiaat bepaald door van der Leeden, van Dalen en de Jonge is niet in overeenstemming met de resultaten van susceptibiliteitsmetingen.

P. van der Leeden, P.A. van Dalen en W.J.M. de Jonge, Physica 33, 202 (1967).
K.Kobayashi en T.Haseda. J.Phys.Soc.Japan 18, 541 (1963).

II

De definitie van N_N, zoals gegeven door Spence en van Dalen, geeft aanleiding tot misverstand, in het bijzonder wanneer het gecenterde roosters betreft.

Dit proefschrift, section 2.2..
R.D.Spence en P.A. van Dalen, Acta Cryst. A24, 494 (1968).

III

De metingen van de elektrische veldgradienten op de deuteriumkernen in $KMnCl_3.2D_2O$ en de resultaten van een berekening van de minimale elektrostatische energie bevestigen globaal de op basis van waterstofbindingen aangenomen kristalwaterposities.

W.J.M. de Jonge, J.P.A.M.Hijmans en E.C.A.Gevers (publicatie in voorbereiding)
J.P.A.M.Hijmans, (intern rapport).

IV

De verhouding van de overgangsfrekwenties van de twee chloorisotopen in de antiferromagnetische fase kan dienen als selectiecriterium voor de tot niet-equivalente chloorposities behorende overgangen.

Dit proefschrift, section 2.4..

V

Het is mogelijk de hoofdassen en asymmetrie-parameter van de elekrische veldgradient tensor op een chloorkern in de niet magnetisch geordende toestand te bepalen, zonder de quadrupool-overgang met een uitwendig magneetveld op te splitsen.

C.H.W.Swüste, W.J.M. de Jonge en W.Harkema (publicatie in voorbereiding).

VI

De door Smith en Friedberg gevonden subrooster-magnetisatierichting in de antiferromagnetische toestand van $CsMnCl_3.2H_2O$ is onjuist.

Dit proefschrift, section 5.4..
T.Smith en S.A.Friedberg, Phys.Rev. 176, 660 (1968).
A.C.Botterman, W.J.M. de Jonge en P. de Leeuw, Phys.Letters 30A, 150 (1969).

VII

Bij de bepaling van de magnetische ruimtegroep van azuriet is geen rekening gehouden met een mogelijke verandering van het Bravaisrooster.

E.P.Riedel en R.D.Spence, Physica 26, 1174 (1960).

VIII

Bij de interpretatie van hun metingen aan de quadrupool-opsplitsing van de deuteriumkernen in $CuSO_4.5D_2O$, houden Soda en Chiba onvoldoende rekening met de invloed van de paramagnetische interactie.

G.Soda en T.Chiba, J.Chem.Phys. 50, 439 (1969).

IX

Alvorens de door Iinuma et al. voorgestelde techniek voor digitale verwerking van radioisotopenscans klinisch toe te passen, zou een onderzoek naar de betrouwbaarheid van de methode wenselijk zijn.

T.A.Iinuma, T.Nagai en N.Fukuda. Proceedings of a symposium on medical radioisotope scintigraphy. Salzburg August 1968.

X

Het ware wenselijk de mogelijkheid van een "sabbatical leave" voor de wetenschappelijke medewerkers aan hoger onderwijs instituten te institutionaliseren. De toekenning van zulk een "verlof" zou gekoppeld moeten worden aan prestatie en te verwachten rendement en als zodanig moeten worden opgenomen in het waarderingssysteem zoals dat aan deze instituten wordt gehanteerd.

Eindhoven, 9 april 1969 W.J.M. de Jonge